nature medicine

A human monoclonal antibody prevents malaria infection by targeting a new site of vulnerability on the parasite

Neville K Kisalu[1,13], Azza H Idris[1,13], Connor Weidle[2], Yevel Flores-Garcia[3], Barbara J Flynn[1], Brandon K Sack[4], Sean Murphy[4], Arne Schön[5], Ernesto Freire[5], Joseph R Francica[1], Alex B Miller[6], Jason Gregory[3], Sandra March[6], Hua-Xin Liao[7,12], Barton F Haynes[7–9], Kevin Wiehe[7,8], Ashley M Trama[7], Kevin O Saunders[7,10], Morgan A Gladden[7], Anthony Monroe[7], Mattia Bonsignori[7,8], Masaru Kanekiyo[1], Adam K Wheatley[1,12], Adrian B McDermott[1], S Katie Farney[1], Gwo-Yu Chuang[1], Baoshan Zhang[1], Natasha Kc[11], Sumana Chakravarty[11], Peter D Kwong[1], Photini Sinnis[3], Sangeeta N Bhatia[6], Stefan H I Kappe[4], B Kim Lee Sim[11], Stephen L Hoffman[11], Fidel Zavala[3], Marie Pancera[2,14] & Robert A Seder[1,14]

Development of a highly effective vaccine or antibodies for the prevention and ultimately elimination of malaria is urgently needed. Here we report the isolation of a number of human monoclonal antibodies directed against the *Plasmodium falciparum* (Pf) circumsporozoite protein (PfCSP) from several subjects immunized with an attenuated Pf whole-sporozoite (SPZ) vaccine (Sanaria PfSPZ Vaccine). Passive transfer of one of these antibodies, monoclonal antibody CIS43, conferred high-level, sterile protection in two different mouse models of malaria infection. The affinity and stoichiometry of CIS43 binding to PfCSP indicate that there are two sequential multivalent binding events encompassing the repeat domain. The first binding event is to a unique 'junctional' epitope positioned between the N terminus and the central repeat domain of PfCSP. Moreover, CIS43 prevented proteolytic cleavage of PfCSP on PfSPZ. Analysis of crystal structures of the CIS43 antigen-binding fragment in complex with the junctional epitope determined the molecular interactions of binding, revealed the epitope's conformational flexibility and defined Asn-Pro-Asn (NPN) as the structural repeat motif. The demonstration that CIS43 is highly effective for passive prevention of malaria has potential application for use in travelers, military personnel and elimination campaigns and identifies a new and conserved site of vulnerability on PfCSP for next-generation rational vaccine design.

Malaria is a mosquito-borne parasitic disease causing high morbidity and mortality primarily in infants and young children in sub-Saharan Africa. Infection with Pf is responsible for the majority of deaths due to malaria. PfCSP covers the surface of the infecting sporozoites and has a critical role in sporozoite development in the mosquito and in the invasion of hepatocytes that is necessary for initiation of malaria infection[1–4]. PfCSP comprises an N-terminal domain, which contains a highly conserved pentapeptide sequence termed region I, that is followed by an immunodominant central repeat region consisting of ~40 NANP motifs and up to 4 NVDP motifs and a C-terminal domain[5,6] (**Fig. 1a**). PfCSP is a major target for neutralizing antibodies, which provided the rationale for using it as a vaccine[7]. High-titer antibodies against the NANP repeats have been associated with some clinical protection following vaccination with RTS,S/ASO1, a truncated formulation of PfCSP containing only NANP repeats and the C-terminal region[8–10]. Moreover, human monoclonal antibodies against the NANP repeats that were isolated from subjects vaccinated with RTS,S/ASO1 protected mice following malaria challenge[11,12]. Of note, antibody levels and protection in humans wane over several years following RTS,S/ASO1 immunization[13,14]. These data highlight the need to induce more durable antibodies with higher potency against NANP repeats or new regions of PfCSP. Heretofore, there are

[1]Vaccine Research Center, National Institute of Allergy and Infectious Diseases, National Institutes of Health, Bethesda, Maryland, USA. [2]Vaccine and Infectious Disease Division, Fred Hutchinson Cancer Research Center, Seattle, Washington, USA. [3]Malaria Research Institute, Johns Hopkins Bloomberg School of Public Health, Baltimore, Maryland, USA. [4]Seattle Biomedical Research Institute, Seattle, Washington, USA. [5]Department of Biology, Johns Hopkins University, Baltimore, Maryland, USA. [6]Division of Health Sciences and Technology, Institute for Medical Engineering and Science, and The Broad Institute, Massachusetts Institute of Technology, Cambridge, Massachusetts, USA. [7]Duke Human Vaccine Institute, Durham, North Carolina, USA. [8]Department of Medicine, Duke University Medical Center, Durham, North Carolina, USA. [9]Department of Immunology, Duke University Medical Center, Durham, North Carolina, USA. [10]Department of Surgery, Duke University School of Medicine, Duke University Medical Center, Durham, North Carolina, USA. [11]Sanaria Inc., Rockville, Maryland, USA. [12]Present addresses: College of Life Science and Technology, Jinan University, Guangzhou, China (H.-X.L.) and Department of Microbiology and Immunology, University of Melbourne, Peter Doherty Institute for Infection and Immunity, Melbourne, Victoria, Australia (A.K.W.). [13]These authors contributed equally to this work. [14]These authors jointly directed this work. Correspondence should be addressed to M.P. (mpancera@fredhutch.org) or R.A.S. (rseder@mail.nih.gov).

Received 22 January; accepted 26 January; published online 19 March 2018; doi:10.1038/nm.4512

limited data characterizing human monoclonal antibodies that bind to sites other than the repetitive NANP motifs and that mediate sterile protection in mice[11,12,15]. Thus, isolation of antibodies from humans exposed to whole sporozoites through vaccination or infection provides a powerful approach for identification of such monoclonal antibodies, as full-length PfCSP is presented in its native conformation. Here we isolated several human monoclonal antibodies specific for PfCSP from subjects immunized with an attenuated whole-sporozoite vaccine (Sanaria PfSPZ Vaccine)[16] and protected against controlled human malaria infection (CHMI)[17]. We then determined the capacity of these antibodies to mediate protection *in vivo* and used structural and biophysical analyses to define their specificity and provide insight into the mechanisms underlying protection.

RESULTS

Isolation of PfCSP monoclonal antibodies from memory B cells and plasmablasts

To isolate PfCSP monoclonal antibodies, two different experimental approaches were used. The first approach used recombinant PfCSP (rPfCSP) and the $(NANP)_9$-repeat peptide as probes to directly identify and sort PfCSP-reactive IgG^+ memory B cells from peripheral blood 2 weeks after the final vaccination (**Fig. 1b**) of a malaria-naive subject who received the PfSPZ vaccine. This immunized subject was protected after CHMI, and serum obtained from this individual had high antibody titers against PfCSP and showed functional inhibition of sporozoite invasion of hepatocytes *in vitro*. Four of the five monoclonal antibodies (CIS23, CIS34, CIS42 and CIS43) showed dose-dependent binding to rPfCSP and PfSPZ in an ELISA and had maximal effective concentrations (EC_{50}s) ranging 0.003–0.134 μg/ml and 0.017–0.08 μg/ml, respectively (**Fig. 1c**). These antibodies also bound PfSPZ in an immunofluorescence assay (**Fig. 1d**). Additional monoclonal antibodies against PfCSP were generated through a second approach using plasmablasts derived from two naive subjects immunized with the PfSPZ vaccine. This method provides a direct and unbiased approach for isolating monoclonal antibodies against PfCSP and other PfSPZ proteins. Plasmablasts were sorted 7 d after the third immunization without any antigen-specific probe, and the sequences encoding immunoglobulin

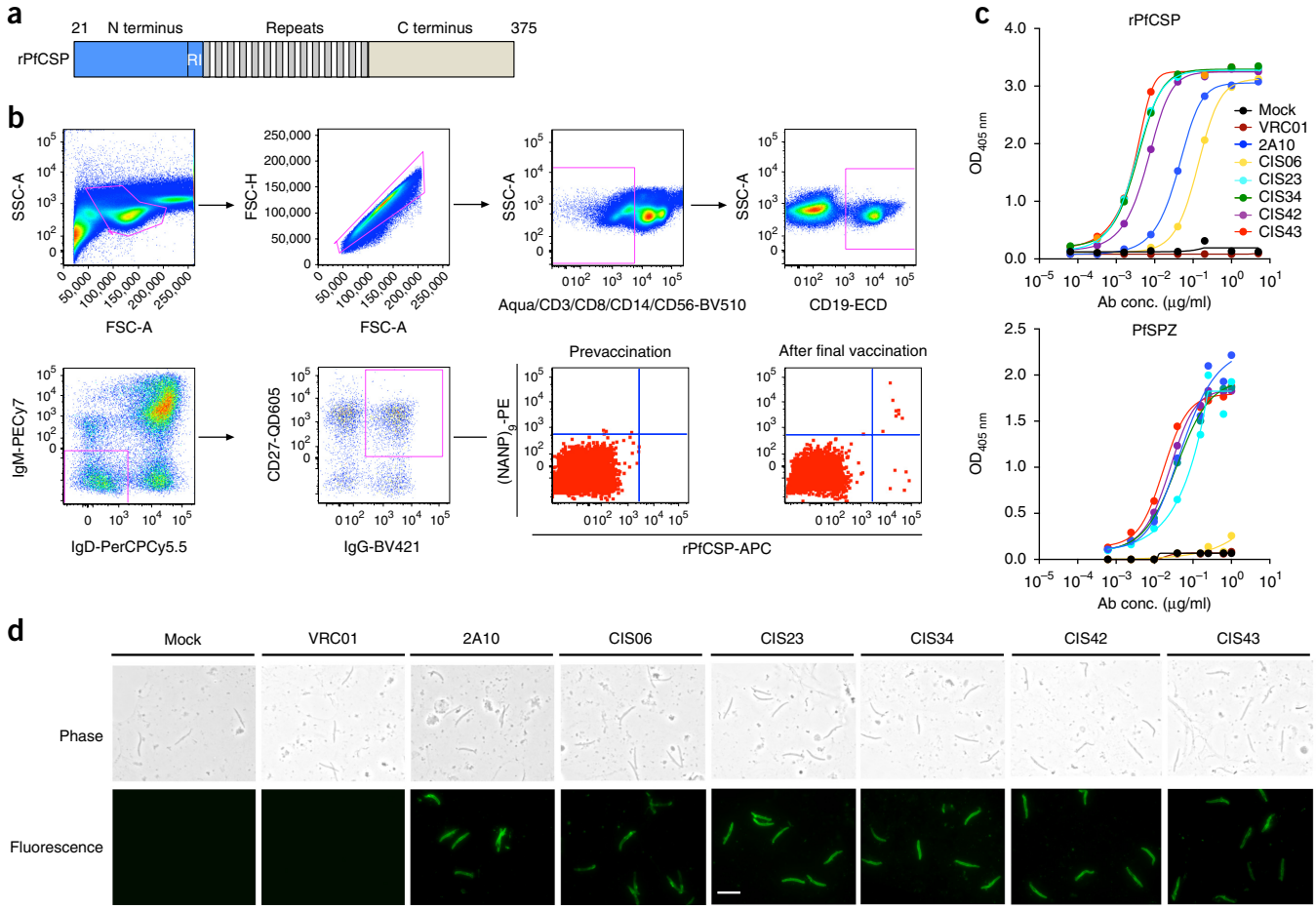

Figure 1 Isolation and binding specificity of monoclonal antibodies from rPfCSP-specific memory B cells. (**a**) Schematic of rPfCSP (residues 21–375). The signal (1–21) and anchor (375–397) residues are excluded. The N-terminal, C-terminal and repeat domains are shown. The conserved region I (RI) is indicated. (**b**) The gating strategy used to sort memory B cells with rPfCSP and the $(NANP)_9$ peptide probes. rPfCSP-specific $CD19^+IgG^+CD27^+$ memory B cells were obtained prevaccination or after the fifth (last) vaccination. (**c**) Top, binding of varying concentrations of monoclonal antibodies to rPfCSP determined through ELISA. $OD_{405\ nm}$, optical density at 405 nm. Bottom, binding of monoclonal antibodies to PfSPZ in an ELISA. (**d**) Binding of monoclonal PfCSP-specific antibodies to PfSPZ as determined through immunofluorescence assay. Phase-contrast and fluorescence channels showing the monoclonal PfCSP-specific antibodies binding to PfSPZ. Scale bar, 10 μm. In **c** and **d**: mock, (negative control), transfection filtrate; VRC01, a human anti-HIV-1 IgG1 isotype control monoclonal antibody[44]. Positive control, 2A10, mouse anti-PfCSP-repeat monoclonal antibody. In **c** and **d**, data are representative of two independent experiments.

heavy chains and light chains were expressed as recombinant antibodies. Of the 141 monoclonal antibodies, 68 were specific for rPfCSP as determined through ELISA; 12 of these antibodies were selected for additional analysis (**Supplementary Fig. 1a**).

The isolated PfCSP-specific monoclonal antibodies utilized distinct heavy and light chain gene families. Comparison between the genes encoding the heavy and light chains and their corresponding germline sequences showed nucleotide identity was 95–100% and 89–100%, respectively. All PfCSP-specific monoclonal antibodies had canonical heavy-chain complementarity-determining region-3 (CDRH3) lengths that ranged 12–17 amino acid residues (**Supplementary Table 1**)[18]. For the PfCSP-specific monoclonal antibodies isolated from plasmablasts, the immunoglobulin heavy variable (*IGVH3*) gene family, and particularly *IGVH3-33*, predominated, which is consistent with recent reports by others[12,15] (**Supplementary Table 1**).

PfCSP-specific monoclonal antibodies inhibit sporozoite infection *in vitro*

The functional inhibitory capacity of the PfCSP-specific monoclonal antibodies was first assessed using an *in vitro* model of Pf liver-stage development in primary human hepatocytes[19,20]. This analysis provides a high-throughput initial screening assay for determining the capacity of hundreds of antibodies in limiting sporozoite invasion of hepatocytes *in vitro* to facilitate downselection for subsequent *in vivo* protection studies. Four of the PfCSP-specific monoclonal antibodies (CIS23, CIS34, CIS42 and CIS43) that were isolated from memory B cells, and three of the PfCSP-specific monoclonal antibodies (mAb04, mAb09 and mAb10) isolated from plasmablasts showed dose-dependent inhibition of sporozoite invasion of hepatocytes (**Supplementary Fig. 1b**).

CIS43 confers sterile protection in two mouse models of malaria infection

Functional inhibition of the PfCSP-specific monoclonal antibodies was then assessed *in vivo* using two different and complementary mouse models of malaria infection. The first model uses a transgenic strain of *Plasmodium berghei* (Pb) in which the endogenous PbCSP has been replaced with the full-length PfCSP (Pb-PfCSP)[21]. Assessment of the PfCSP-specific monoclonal antibodies can be undertaken in the context of a natural infection in C57BL/6 mice, as these mice are permissive for Pb infection. In this model, we first infected mice via intravenous injection and determined the capacity of the PfCSP-specific antibodies to mediate reduction of liver-stage parasite burden. This direct inoculation is a stringent assessment of antibody function and provides a dynamic range for comparing the relative inhibitory capacity of the antibodies. Passive transfer of the monoclonal antibody CIS43 in mice following intravenous infection led to the highest reduction (~2–4 logs) of the liver-stage parasite burden in a dose-dependent manner ($P < 0.008$; **Fig. 2a**,**b**) as compared to the liver-stage parasite burden in untreated mice or those receiving transfection filtrate (mock); the second-highest reduction was observed following transfer of CIS34, which led to a ~2-log reduction ($P < 0.008$; **Fig. 2a**). We then assessed the inhibitory capacity of the three monoclonal antibodies (mAb04, mAb09 and mAb10) isolated from plasmablasts that showed *in vitro* inhibition (**Supplementary Fig. 1b**). Of these antibodies, liver-stage parasite burden was most significantly reduced (~1–2 log) in mice treated with mAb10 as compared to untreated mice ($P < 0.008$; **Fig. 2b**). In all four experiments, CIS43 showed significantly better protection than 2A10, a mouse monoclonal antibody specific for the repeat region of PfCSP[22,23], or mAb10 ($P < 0.008$, two-tailed Mann-Whitney test; **Fig. 2a**,**b**). Of note, CIS42, mAb04 and mAb09, which all had potent inhibitory activity *in vitro*, did not significantly reduce liver-stage parasite burden *in vivo* (**Fig. 2a**,**b**). These data are consistent with prior reports showing similar differences using serum from immunized subjects[24,25] and highlight the importance of *in vivo* studies for demonstrating protective efficacy.

As malaria infection is naturally transmitted through mosquito bites, and antibodies to PfCSP have inhibitory effects in the skin[26], the protective capacity of the PfCSP-specific monoclonal antibodies was further assessed in C57BL/6 mice challenged with infectious mosquito bites. In two independent experiments, all 14 mice that received CIS43, 13 of 14 mice that received CIS34 and 7 of 7 mice that received mAb10 were free of parasites in blood up to 12 d after infection ($P = 0.0001$, log-rank test). In contrast, only 2 of 7 mice that received 2A10 were parasite-free (**Fig. 2c**). Last, serum antibody levels following passive transfer were approximately 150–200 μg/ml for all PfCSP-specific monoclonal antibodies (**Fig. 2d**). These data show that differences in protective efficacy of the monoclonal antibodies *in vivo* are likely related to binding specificity and affinity rather than differing amounts of antibody *in vivo*.

To substantiate the *in vivo* protective capacity of PfCSP-specific monoclonal antibodies in another mouse model, we used human liver-chimeric (FRG-huHep) mice that were permissive to infection with Pf[27]. Considering the limited availability of these mice, our studies focused on CIS43, which was consistently the most protective antibody *in vivo* (**Fig. 2a**,**b**). In the first experiment following passive transfer of CIS43, mice were exposed to 50 infected mosquitoes. This model of high-dose challenge provides a dynamic range for assessment of reduction in parasite load in liver as a first demonstration of protection. As compared to the mice treated with a mock control monoclonal antibody, there was a dose-dependent reduction ($P = 0.001$ and $P = 0.041$, respectively) of Pf burden in liver of 80–90% following treatment with CIS43 (**Fig. 2e**). We then exposed mice to five infected mosquitoes and transferred human red blood cells into these mice to assess sterile protection in blood. Of note, this challenge with five infected mosquitoes is similar to that used for CHMI following vaccination in human clinical trials[28,29]. In two independent experiments, 10 of 15 mice were free of parasites in blood ($P = 0.0002$) following passive transfer of only 50 μg of CIS43 (**Fig. 2f**) with serum levels of the antibody that were ~10 μg/ml at the time of mosquito challenge (**Fig. 2g**). Collectively, these data show that CIS43 conferred high-level, sterile protection in two mouse models of malaria infection.

CIS43 preferentially binds to a unique junctional epitope between the N terminus and central repeat domains of PfCSP

To understand the mechanisms underlying the differential *in vivo* potency of the PfCSP-specific monoclonal antibodies, binding analysis via mapping to PfCSP was performed. Binding specificity was first assessed against polypeptides representing the N-terminal, central repeat and C-terminal regions. All PfCSP-specific monoclonal antibodies that were tested for *in vivo* function bound only within the central repeats, highlighting the immunodominance of this region of PfCSP following vaccination with the PfSPZ vaccine (**Supplementary Fig. 1c**). More detailed mapping of PfCSP-specific monoclonal antibodies was performed using a series of linear peptides that were 15 amino acids in length, overlapping by 11 amino acids encompassing the central repeat region (peptides 20–61, residues 97–276; **Fig. 3a** and

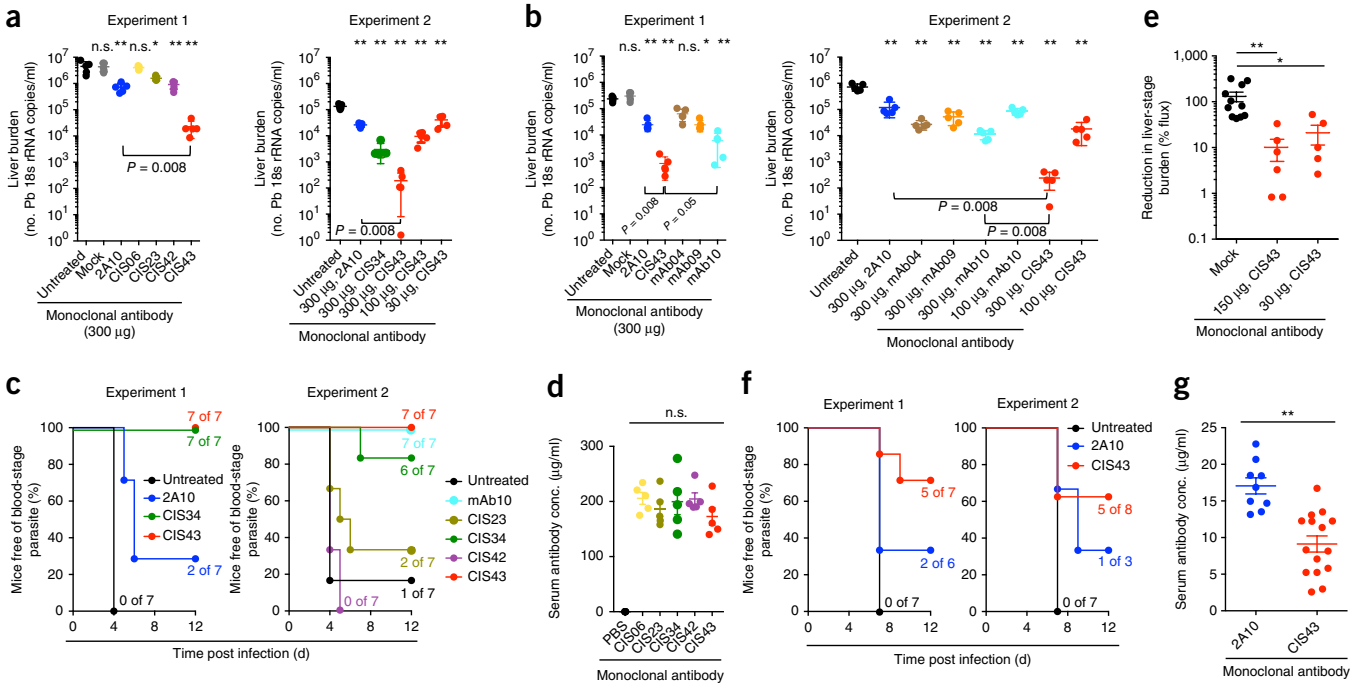

Figure 2 PfCSP-specific monoclonal antibodies provide protection against malaria infection. (**a**,**b**) PfCSP-specific monoclonal antibodies isolated from rPfCSP-specific memory B cells (**a**) and plasmablasts (**b**) have a protective effect against liver-stage parasite burden in C57BL/6 mice ($n = 5$ mice per group) that were challenged intravenously (i.v.) with Pb-PfCSP. Liver-stage parasite burden is expressed as the number of Pb 18s ribosomal RNA (rRNA) copies per ml of liver tissue homogenate, and the difference between each antibody and the untreated group was determined using the two-tailed Mann–Whitney test. $^{*}P = 0.016$, $^{**}P = 0.008$. n.s., not significant. The brackets reflect comparisons between CIS43 and 2A10 or mAb10. (**c**) PfCSP monoclonal antibodies provide sterile protection following Pb-PfCSP SPZ infection via mosquito bite. C57BL/6 mice were challenged with five infected mosquitoes following passive transfer (300 µg) of the indicated monoclonal antibodies. Kaplan–Meier curves, analyzed using the log-rank test, show the frequencies of mice free of parasites as determined through Giemsa staining of blood. Differences between CIS43-, CIS34- and mAb10-treated mice and untreated mice were significant ($P = 0.0001$) ($n = 7$ mice per group per experiment). (**d**) Serum levels of PfCSP-specific monoclonal antibodies 1 h after passive transfer of 300 µg of the indicated monoclonal antibodies as determined through ELISA from a separate experiment using C57BL/6 mice ($n = 5$ mice per group). Differences in monoclonal antibody levels were compared for significance using a one-way ANOVA with Dunnett's correction for multiple comparisons. (**e**) Protective effect of monoclonal antibody CIS43 against liver-stage parasite burden following Pf infection in FRG-huHep mice that were challenged with 50 mosquitoes infected with Pf expressing GFP–luciferase. Parasite burden was determined 6 d following challenge using bioluminescent imaging (flux in pixels/second). Results were normalized to those from mice that received a nonspecific IgG (mock). Mock, $n = 12$ mice; 150 and 30 µg CIS43, $n = 7$ and 6 mice, respectively. The Kruskal–Wallis test with Dunn's correction was used for multiple comparisons. $^{*}P = 0.041$, $^{**}P = 0.001$. (**f**) PfCSP monoclonal antibodies provide sterile protection following PfSPZ infection. Following passive transfer (50 µg) of the indicated monoclonal antibodies, FRG-huHep mice were challenged with 5 infected mosquitoes. Kaplan–Meier curves, analyzed using the log-rank test, show the frequencies of mice free of parasites as determined by the number of Pf 18s rRNA copies per ml of blood on day 7 and 9. In both experiments, mice treated with CIS43 were significantly more protected than untreated mice ($P = 0.0002$). CIS43, $n = 15$ mice; 2A10, $n = 9$ mice; untreated, $n = 14$ mice, respectively. (**g**) Serum levels of PfCSP-specific monoclonal antibodies in the FRG-huHep mice used in **f** were assessed at the time of challenge. Data were compared for significance using the two-tailed Mann–Whitney test. $^{**}P = 0.001$. In **d** and **e**, data are representative of two independent experiments, and the bar denotes the geometric mean, and error bars denote the s.e.m. In **a**, **b** and **g**, the median is shown with standard error. Each dot represents one mouse.

Supplementary Fig. 1d,**e**). This showed that PfCSP-specific monoclonal antibodies isolated from plasmablasts bound only NVDP and NANP repeats (**Supplementary Fig. 1e**). In striking contrast, CIS43 showed potent binding to peptide 20 (^{97}PADGNPDPNANPNVD^{111}) and peptide 21 (^{101}NPDPNANPNVDPNAN^{115}) with an $EC_{50} < 0.0001$ µg/ml and reduced binding to the representative NANP-repeat peptide 29 (^{132}NANPNANPNANPNAN^{147}) with an $EC_{50} > 5.0$ µg/ml (**Fig. 3a** and **Supplementary Fig. 1d**). Furthermore, preincubation of CIS43 with peptides 20 or 21 inhibited binding to rPfCSP in a dose-dependent manner (**Fig. 3b**) with IC_{50} values of 4.4 µg/ml or 0.29 µg/ml, respectively. This striking capacity of peptide 21 to inhibit binding of CIS43 to rPfCSP was not observed with the other PfCSP-specific monoclonal antibodies (**Fig. 3b** and **Supplementary Fig. 1e**,**g**). Peptide 21 is a unique region at the junction of the N terminus and the central repeat domains that we define here as the junctional epitope.

Alanine scanning mutagenesis of peptide 21 was done to define the residues that are critical for the binding of CIS43 to rPfCSP. If an alanine occurred in the original sequence, it was substituted with an arginine, glycine, proline, serine or valine (**Fig. 3c**). The N107A (**Fig. 3c**, second panel, orange), P108A (**Fig. 3c**, second panel, green) or N109A (**Fig. 3c**, third panel, blue) substitution abrogated the capacity of peptide 21 to compete with CIS43 for binding to rPfCSP and PfSPZ (**Fig. 3c**,**d**). Moreover, peptide 25, which is identical to peptide 21 except for the P102V substitution, had a lower inhibitory capacity than peptide 21 ($IC_{50} = 36.7$ µg/ml and $IC_{50} = 0.29$ µg/ml, respectively), suggesting a key role for Pro102 in the interaction between peptide 21 and CIS43 (**Fig. 3b**,**c**).

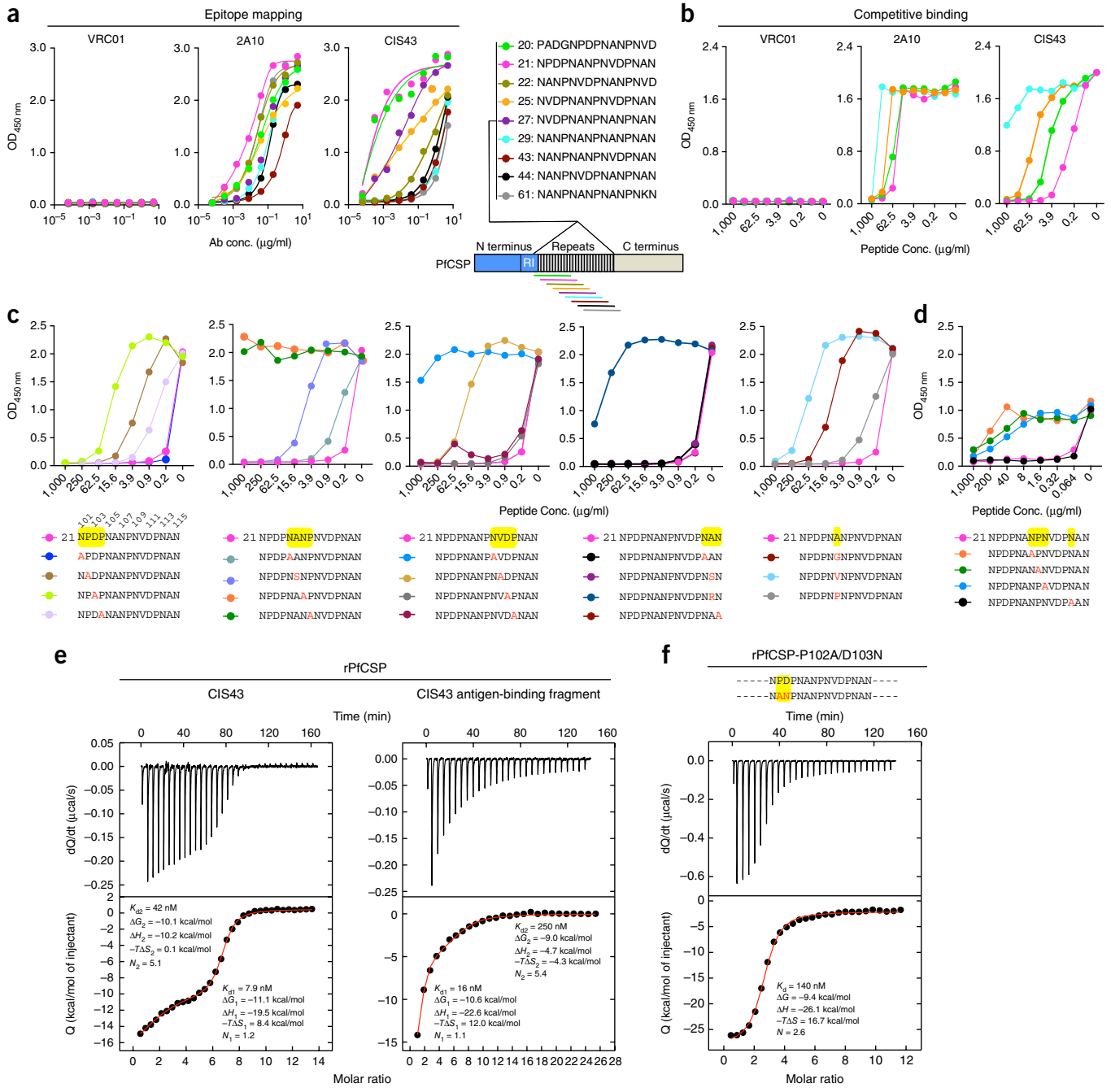

Figure 3 Epitope mapping and ITC analysis of CIS43. (**a**) Left, CIS43 binding to overlapping peptides of PfCSP. Binding of peptides to control antibodies VRC01 (isotype-matched, negative control human anti-HIV-1) and 2A10 (positive control mouse repeat–specific PfCSP) are also shown. Right, specified amino acid sequences numbered 20–61 are shown. Sequences are color-coded, representing overlapping peptides spanning the repeat region of PfCSP (residues 97–276). Peptides 28–41 and 46–60 consisted only of NANP repeats and are represented by peptide 29. (**b**) CIS43 binding to rPfCSP in the presence of varying concentrations of peptides. VRC01 and 2A10 were use as controls and peptides are color-coded as in **a**. (**c**) Top, CIS43 binding to rPfCSP in the presence of peptide 21 sequence variants. Bottom, the wild-type peptide 21 sequence is shown (pink), as are several sequences with variants. The numeric position is listed above each residue and is shown only in the first panel. The residues highlighted in yellow indicate the native sequence at that position, and the resulting mutations are shown in red. (**d**) Top, binding of CIS43 to PfSPZ in the presence of peptide 21 and its sequence variants. Bottom, the wild-type peptide 21 sequence is shown (pink), as are several sequences with variants. (**e**,**f**) Results from ITC analysis of binding between monoclonal antibody CIS43 and rPfCSP and between the CIS43 antigen-binding fragment and rPfCSP (**e**) and of binding between monoclonal antibody CIS43 and a PfCSP mutant with the P102A and D103N substitutions; changes in the junctional epitope sequence are depicted in red and highlighted in yellow. (**f**) Top, the output signal, dQ/dt, which equals the heat flow is shown as a function of time. Bottom, the integrated heat associated with each injection (Q) is shown as a function of the molar ratio between the antigen-binding fragment site and rPfCSP in the cell. The solid line represents the result from best nonlinear least squares fit of the data to a binding model that takes into account two sets of sites with different affinities for rPfCSP. Data shown are representative of three independent experiments. The dissociation constant (K_d), change in Gibbs energy (ΔG) of binding, enthalpy (ΔH), the entropy contribution to Gibbs energy ($-T\Delta S$) and stoichiometry (N) are shown. In **a**–**e**, data are representative of two independent experiments.

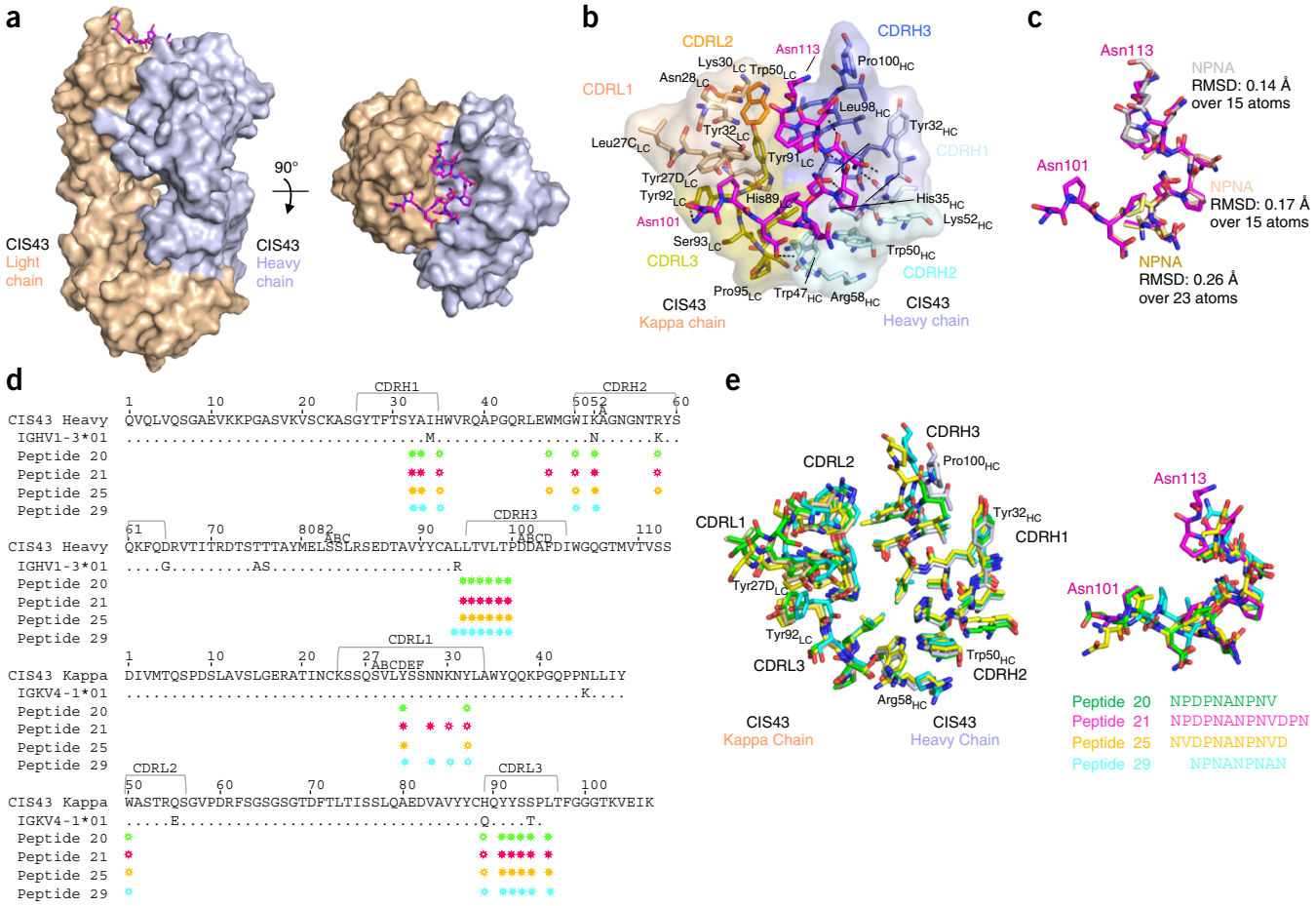

Figure 4 Crystal structures of the CIS43 antigen-binding fragment in complex with PfCSP peptides. (**a**) Left, a surface representation of the CIS43 antigen-binding fragment (light chain in tan and heavy chain in light blue) is shown, with peptide 21 ^{101}NPDPNANPNVDPN^{113} from the repeat region of PfCSP shown in sticks (purple). Right, a 90° rotation of the representation with view down toward the combining sites is shown. (**b**) Details of the interactions between peptide 21 and the CIS43 antigen-binding fragment. Purple sticks depict peptide 21. The semitransparent surface represents the CIS43 epitope, and the colored sticks represent the amino acids comprising this epitope. Residues are colored on the basis of the CDR region they belong to; residues in the light chain (LC) are shown in tan or yellow, and residues in the heavy chain (HC) are shown in light or dark blue. (**c**) A stick representation of peptide 21 (purple) is shown in the conformation bound to CIS43 with superposition of three NPNA repeat structures of CSP with a β-1 turn as described by Ghasparian *et al.*[33] Each NPNA repeat is labeled for clarity and shown in different colors. Root mean square deviation (RMSD) is indicated over the total number of atoms used in the alignment. (**d**) Sequence of the CIS43 antigen-binding fragment following Kabbat numbering and alignment with the amino acid sequence encoded by the variable germline gene sequence. Residues that contact each peptide (green, red, yellow and blue for peptide 20, 21, 25 and 29, respectively) are shown as an open star for side chains only and a closed star for both main and side chains. (**e**) Left, detailed representation of the interactions of the peptides with the CIS43 antigen-binding fragment. Residues within 5 Å of the peptides are shown as sticks in tan for the light chain residues and in blue for the heavy chain residues when bound to peptide 21 and as green, yellow and cyan for peptide 20, peptide 25 and peptide 29, respectively. Right, superposition of the peptides shown as sticks. Peptides are colored as in **d** with sequences noted for the residues observed in electron density.

CIS43 shows sequential, multivalent, high-affinity binding to PfCSP

In the first assessment for affinity using biolayer inferometry, CIS43 had the highest apparent affinity (<0.001 nM) to peptide 21 as compared to that of the other PfCSP-specific monoclonal (range, <0.001–6.06 nM; **Supplementary Fig. 2** and **Supplementary Table 2**). These results are consistent with the epitope mapping data (**Fig. 3a**,**b**). Thermodynamic parameters and stoichiometry of binding between CIS43, CIS42, CIS23, CIS34 and mAb10 to rPfCSP were then determined using isothermal titration calorimetry (ITC). Remarkably, IgG and the antigen-binding fragment of CIS43 each showed two sequential binding events to rPfCSP: the first involved a single binding site per antibody with an affinity of 7.9 nM and 16 nM, respectively, and the second involved five binding sites with an affinity of 42 nM and 250 nM, respectively (**Fig. 3e**)[30]. Similarly, CIS34 also had two binding events, with one site bound with an affinity of 31 nM and eight other sites bound with an affinity of 80 nM (**Supplementary Fig. 3**). In contrast, CIS23, CIS42 and mAb10 had only one binding event, with 6, 7 or ~9 binding sites with an affinity of 25 nM, 51 nM or 27 nM, respectively (**Supplementary Fig. 3**); this is consistent with recent reports using other mouse and human monoclonal antibodies against the NANP-repeat epitopes[12,31]. To further understand the sequential binding event observed for CIS43, we performed ITC analysis of binding between CIS43 and peptide 21, peptide 29 or a mutant form of rPfCSP. Binding between CIS43 and peptide 21 had an affinity of 7.5 nM, and the affinity was 53 nM between CIS43 and peptide 29 (**Supplementary Fig. 3b**). These are similar to values obtained using rPfCSP, suggesting that the first binding event is to

peptide 21. Additionally, ITC analysis using CIS43 and a mutant PfCSP, in which two unique residues specific for the junctional epitope were mutated (P102A and D103N), indicated that only one multivalent binding event occurred, with a reduced affinity of 140 nM and a stoichiometry of three binding sites (**Fig. 3f**). The binding affinity and stoichiometry between mAb10, which was used as a control and does not bind peptide 21, and the mutant PfCSP was not different as compared to rPfCSP (**Supplementary Fig. 3c**). These data strongly suggest that the first high-affinity binding event between CIS43 and rPfCSP occurs at the junctional epitope and that such binding may induce conformational changes of rPfCSP, which can influence the stoichiometry of the remaining binding events of CIS43.

Crystal structures of the antigen-binding fragment of CIS43 in complex with multiple PfCSP peptides

Attempts to co-crystallize rPfCSP with CIS43 were unsuccessful, likely owing to the multivalent stoichiometry of antibody binding to rPfCSP and the flexibility of this protein[32]. To determine the molecular interactions of epitope binding to CIS43, we co-crystallized the CIS43 antigen-binding fragment with peptides 20, 21, 25 and 29, as these peptides differentially competed with binding to rPfCSP (**Fig. 3b**). Crystals were obtained that diffracted X-rays to 2.4 Å, 1.8 Å, 2.0 Å and 2.2 Å with peptides 20, 21, 25 and 29, respectively (**Supplementary Table 3**). The peptides inserted into a hydrophobic groove that formed at the interface of the heavy and light chains, which is positively charged and tyrosine-rich and involved all the complementarity-determining regions (CDRs; **Fig. 4a**,**b**,**d**, **Supplementary Fig. 4** and **Supplementary Table 4**). Some conformational changes were observed: residues Tyr32, Trp50, Lys52, Arg58 and Pro100 of the heavy chain and residues Tyr27, Asn28, Tyr32, Trp50, Tyr91 and Tyr92 of the light chain showed movement when bound to different peptides (**Fig. 4e**, left panel). Although peptides 20, 21 and 25 adopted a similar overall conformation (except at the N terminus of peptide 25 and at all of the C termini; **Fig. 4e**, right panel), peptide 29 adopted a different conformation. CIS43 has low affinity maturation (**Fig. 4d** and **Supplementary Table 1**). Four of the eleven somatically mutated residues encoded within the variable-region of the heavy and the light chains interact with the epitope (**Fig. 4d** and **Supplementary Table 4c**,**d**). The β-1 turn conformation, defined previously for the ANPNA peptide[33,34], was observed in the structures composed of bound peptide and antibody, and three β-1 turns could be aligned consecutively to peptide 21 (**Fig. 4c**). We note that the peptides did not adopt the helical stem-like conformation reported previously[32] (**Fig. 4d** and **Supplementary Table 4**). To confirm which of the CIS43 residues mediate binding to peptide 21, variants of this antibody were generated. One variant (with N56G, T57G, R58G and E61G in the heavy chain; **Supplementary Fig. 5a**) abrogated binding to peptide 21 (**Supplementary Fig. 5b**). Of note, Arg58 in the heavy chain of CIS43 was shown to be a key residue for binding to peptide 21 through structural analysis (**Fig. 4**). Moreover, computational free energy calculations revealed R58G to be the most important of all four mutants for peptide binding (**Supplementary Fig. 5c**). Notably, this antibody variant exhibited minimal binding to rPfCSP and no functional inhibition of PfSPZ invasion *in vitro* (**Supplementary Fig. 5b**,**d**).

Crystal structures of the antigen-binding fragment of CIS42 in complex with multiple PfCSP peptides

To further understand the relative functional potency of CIS43, we cocrystallized the antigen-binding fragment of CIS42, which has limited *in vivo* function (**Fig. 2a,c**), with the same peptides (20, 21, 25 and 29) and obtained crystals that diffracted X-rays to resolutions of 2.4 Å, 1.8 Å, 2.0 Å and 2.2 Å, respectively (**Supplementary Fig. 6** and **Supplementary Table 5**). The structures show that, unlike what occurred with the antigen-binding fragment of CIS43, all four peptides adopted an almost identical conformation when bound to the antigen-binding fragment of CIS42; peptide 29 exhibited the most contacts with the CIS42 antigen-binding fragment (**Supplementary Fig. 6**). These data are in accordance with results from the peptide competition analysis of CIS42 (**Supplementary Fig. 1c**). Additionally, the conformation of peptide 21 differed when bound to the antigen-binding fragments of CIS42 or CIS43, and the angles of approach of these antibodies to the peptide also differed (**Supplementary Fig. 7**).

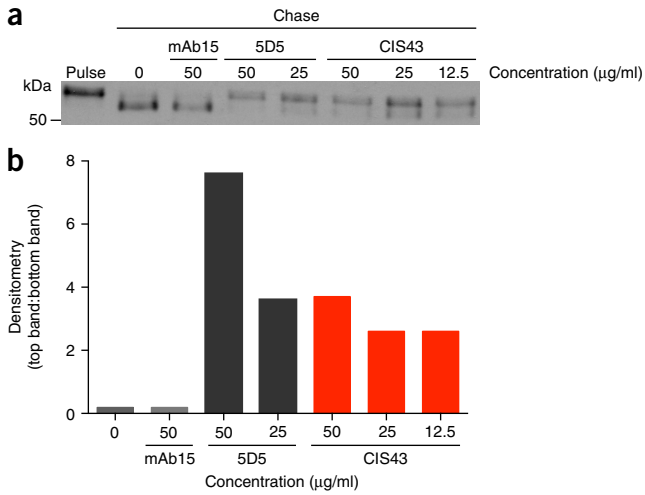

Figure 5 Monoclonal antibody CIS43 affects cleavage of PfCSP on PfSPZ. (**a**) Metabolically labeled Pf sporozoites were kept on ice (pulse) or chased for 90 min in the absence or presence of the indicated concentrations of monoclonal antibodies. PfCSP was immunoprecipitated from sporozoite lysates and analyzed using SDS-PAGE and autoradiography. Negative control, mAb15 (anti–C terminus PfCSP; **Supplementary Fig. 1c**). Positive control, 5D5 (mouse antibody specific for the N terminus of PfCSP)[37]. (**b**) Results from densitometry analysis of the scanned autoradiograph shown in **a**. The density ratio of the top PfCSP band to the bottom PfCSP band is shown for each chased sample at the indicated monoclonal antibody concentration. A ratio of 1 indicates the density of the top and bottom bands is equal. All data are representative of 3 independent experiments.

Molecular dynamics simulation of peptide 21 with CIS43 and CIS42 antigen-binding fragments

Molecular dynamics simulations were then used to further analyze the physical movements and stability of CIS43 and CIS42 bound to peptide 21 (**Supplementary Fig. 8a–c**). After 500 ns, peptide 21 remained buried in the hydrophobic groove of the complementarity-determining region of CIS43, whereas it detached from its initial binding pocket in CIS42 and lost most of its electrostatic interactions, confirming the clear preference of CIS43 for this epitope (**Supplementary Fig. 8d,e** and **Supplementary Videos 1–3**). Principal component analysis (PCA) of results from peptide 21 molecular dynamics simulation showed that CIS43 binds to a rare conformation of peptide 21 (**Supplementary Fig. 8f**).

Definition of NPN as the structural repeat motif of PfCSP

Lastly, as this is the first time to our knowledge that structures of multiple PfCSP motifs are reported, we sought to define the repeat structure

in PfCSP. The analysis showed that Ramachandran angles with antibody-bound repeat peptides had similar phi and psi angles at every four residues, with a few notable outliers (**Supplementary Fig. 9**). These data substantiated the notion that NPN is the structural repeat that defines PfCSP sequences that contain NANP[12,34,35].

CIS43 inhibits cleavage of PfCSP

A key requirement for sporozoite infection of hepatocytes is the proteolytic cleavage of PfCSP at the putative processing site region I[36,37], which is located only three amino acids upstream of the junctional epitope. Thus, to gain additional insight into the mechanism underlying how CIS43 could mediate protection, we assessed whether CIS43 could affect processing or cleavage of PfCSP. Metabolically labeled PfSPZs were chased in the presence of CIS43. We used 5D5, a mouse monoclonal antibody specific for an epitope upstream of region I that has been shown to block cleavage[37], as a positive control. Additionally, mAb15, which is specific for the C terminus of PfCSP (**Supplementary Fig. 1**), was used as a negative control. Indeed, CIS43 did limit cleavage of PfCSP in a dose-responsive manner, albeit to a lesser extent than 5D5 (**Fig. 5** and **Supplementary Fig. 10**).

DISCUSSION

Here we show that the human monoclonal antibody CIS43 binding to a structurally defined junctional epitope on PfCSP confers high-level, sterile protection *in vivo*. Biophysical and structural analyses showing sequential and multivalent high-affinity binding of CIS43 to rPfCSP demonstrated a unique mechanism for neutralization of the parasite. Moreover, binding of CIS43 at a specific angle to a rare conformation of the junctional epitope (**Supplementary Figs. 7** and **8**) highlights how the immunodominant NANP sequence, now structurally defined as NPN, may potentially shield the NPDP junctional site from recognition and thus may divert the immune response away from this site or other sites of vulnerability (**Fig. 3c–f**). Indeed, this unique NPDP sequence is critical for the high-affinity binding of CIS43 to the junctional epitope and may play a role in the overall conformation of rPfCSP for the sequential, multivalent binding of CIS43 (**Fig. 3e**,**f**). We speculate that CIS43 has multiple mechanisms for mediating protection *in vivo*. Multivalent binding of CIS43 to PfCSP could inhibit sporozoite motility in the skin[26]. In addition, through interfering with cleavage of PfCSP, this monoclonal antibody could limit invasion of hepatocytes by sporozoites[36].

There are two potential clinical applications of the findings reported here. One is related to using monoclonal antibodies as passive prevention and the other is using the junctional epitope as part of a next-generation vaccine. As the junctional epitope sequence of CIS43 occurs only once in PfCSP and is highly conserved (>99.8%) amongst thousands of Pf strains recovered globally (see URLs; **Supplementary Fig. 11**)[38–42], it provides a conserved site for antibody neutralization through passive transfer and vaccine design to induce production of such antibodies. The most critical features for conferring protection through passive transfer of monoclonal antibodies or vaccine-induced immunity is potency and durability. The findings that CIS43 leads to a 10- to 100-fold reduction in the burden of parasites at the liver- stage as compared to mAb10, an antibody against the NANP-repeat region only (**Fig. 2b**), provides evidence for greater potency of CIS43. Additional studies comparing CIS43 and other newly identified human monoclonal antibodies against PfCSP that bind to NANP[12,15] will need to be performed to broaden these findings. The ability of CIS43 to protect against Pf infection in the majority of mice at a concentration of ~10 μg/ml *in vivo* is notable because this concentration is achievable for up to 6 months using subcutaneous immunization with a human monoclonal antibody specific to a protein in the HIV envelope[43]. These data suggest that CIS43 could be used alone or in combination with other antibodies for passive prevention in humans in whom high-level protection would be required for up to 6 months. Such a regimen could be used by travelers and military personnel and in elimination campaigns in combination with mass administration of antimalarial drugs. Finally, this junctional epitope provides a new and conserved site of vulnerability for inducing CIS43 like antibodies. The limited affinity maturation of CIS43 from the germline sequence of the gene encoding the variable region suggests that induction of this type antibody may be readily achievable with structure or epitope-based vaccine design. Such next-generation subunit vaccines that increase the breadth and potency of humoral immunity should improve protective efficacy against malaria.

URLs. The Pf3K Project: pilot data release 5, http://www.malariagen.net/data/pf3k-5/.

METHODS

Methods, including statements of data availability and any associated accession codes and references, are available in the online version of the paper.

Note: Any Supplementary Information and Source Data files are available in the online version of the paper.

ACKNOWLEDGMENTS

We thank the study volunteers from the malaria clinical trials VRC312 and VRC314. We thank R. Bailer (Vaccine Research Center, National Institutes of Allergy and Infectious Diseases, National Institutes of Health), for providing peripheral blood mononuclear cell samples. We thank R. Lynch, S. Narpala, M. Prabhakaran, R. Nguyen and X. Chen (Vaccine Research Center, National Institutes of Allergy and Infectious Diseases, National Institutes of Health) for technical help and advice regarding the experiments. We thank I. Cockburn (Australian National University College of Health and Medicine) for providing some of the biotinylated $(NANP)_9$ probe used here. We thank T. Zhou (Vaccine Research Center, National Institutes of Allergy and Infectious Diseases, National Institutes of Health) for providing monoclonal antibody VRC01. We thank C. Peckels, A. Foulger, A. Holland and M. Wang (Duke Human Vaccine Institute (DHVI)) for technical assistance and H. Bouton-Verville (DHVI) for project management. We are grateful to C. A. Schramm's expertise and assistance in analyzing the malaria Pf3K database. We thank the Sanaria Manufacturing Team for the production of fresh PfSPZ. We thank M. Nason for technical help with statistical analysis. We thank B. Graham (Vaccine Research Center, National Institutes of Allergy and Infectious Diseases, National Institutes of Health) for insightful discussion regarding the project. We are particularly grateful to L. Stamatatos for use of laboratory space and equipment. We thank the J. B. Pendleton Charitable Trust for its generous support of Formulatrix robotic instruments. This work was supported by the National Institutes of Health grant GM56550 and the National Science Foundation grant MCB-1157506 to E.F. M.P. and C.W. were supported by a Vaccine and Infectious Disease Division Faculty Initiative Grant through the Fred Hutchinson Cancer Research Center. X-ray diffraction data was collected at the Berkeley Center for Structural Biology beamlines 5.0.1 and 5.0.2, which are supported in part by the National Institute of General Medical Sciences, National Institutes of Health. The Advanced Light Source is supported by the Director, Office of Science, Office of Basic Energy Sciences, of the United States Department of Energy under contract number DE-AC02-05CH11231. Work done at Duke Universiy has been funded in part with Federal funds from the National Cancer Institute, National Institutes of Health, under Contract No. HHSN261200800001E. Production and characterization of the PfSPZ Vaccine were supported in part by the National Institute of Allergy and Infectious Diseases Small Business Innovation Research Grants 5R44AI058375-08 (to S.L.H.).

The findings and conclusions in this report are those of the authors and do not necessarily reflect the views of the funding agency or collaborators. The views expressed in this publication are those of the authors and do not necessarily reflect

the official policy or position of the Department of Health and Human Services or the United States Government.

AUTHOR CONTRIBUTIONS

N.K.K., A.H.I., B.K.S., M.P., F.Z. and R.A.S. planned the studies. N.K.K., A.H.I., B.K.S., S. Murphy, C.W., Y.F.-G., B.J.F., A.S., J.R.F., S. March, A.B.M., M.K., A.K.W., S.K.F., G.-Y.C., S.C., N.K., B.Z., J.G., P.S. and M.P. conducted experiments. F.Z. provided mouse monoclonal antibodies 2A10 and 5D5. K.W., K.O.S., A.M.T., M.A.G. and A.M. contributed new methodologies, analytic tools and performed research. M.B., H.-X.L. and B.F.H. isolated, cloned and produced plasmablast antibodies and analyzed data. N.K.K., A.H.I., B.K.S., F.Z., S.H.I.K., S.C., A.S., E.F., S. March, A.B.M., P.D.K., P.S., S.N.B., B.K.L.S., S.L.H., M.P. and R.A.S. interpreted results from the studies. N.K.K., A.H.I., M.P. and R.A.S. wrote the paper. All authors reviewed, edited and approved the paper.

COMPETING INTERESTS

N.K., S.C., B.K.L.S. and S.L.H. are salaried employees of Sanaria Inc., the developer and owner of the PfSPZ Vaccine and the sponsor of the clinical trials. In addition, S.L.H. and B.K.L.S. have a financial interest in Sanaria Inc. All other authors declare no competing financial interests.

1. Ménard, R. *et al.* Circumsporozoite protein is required for development of malaria sporozoites in mosquitoes. *Nature* **385**, 336–340 (1997).
2. Coppi, A. *et al.* Heparan sulfate proteoglycans provide a signal to *Plasmodium* sporozoites to stop migrating and productively invade host cells. *Cell Host Microbe* **2**, 316–327 (2007).
3. Ancsin, J.B. & Kisilevsky, R. A binding site for highly sulfated heparan sulfate is identified in the N terminus of the circumsporozoite protein: significance for malarial sporozoite attachment to hepatocytes. *J. Biol. Chem.* **279**, 21824–21832 (2004).
4. Rathore, D., Sacci, J.B., de la Vega, P. & McCutchan, T.F. Binding and invasion of liver cells by *Plasmodium falciparum* sporozoites. Essential involvement of the amino terminus of circumsporozoite protein. *J. Biol. Chem.* **277**, 7092–7098 (2002).
5. Dame, J.B. *et al.* Structure of the gene encoding the immunodominant surface antigen on the sporozoite of the human malaria parasite *Plasmodium falciparum*. *Science* **225**, 593–599 (1984).
6. Enea, V. *et al.* DNA cloning of *Plasmodium falciparum* circumsporozoite gene: amino acid sequence of repetitive epitope. *Science* **225**, 628–630 (1984).
7. Nussenzweig, R.S. & Nussenzweig, V. Antisporozoite vaccine for malaria: experimental basis and current status. *Rev. Infect. Dis.* **11** (Suppl. 3), S579–S585 (1989).
8. Casares, S., Brumeanu, T.D. & Richie, T.L. The RTS,S malaria vaccine. *Vaccine* **28**, 4880–4894 (2010).
9. White, M.T. *et al.* The relationship between RTS,S vaccine-induced antibodies, CD4$^+$ T cell responses and protection against *Plasmodium falciparum* infection. *PLoS One* **8**, e61395 (2013).
10. Stoute, J.A. *et al.* A preliminary evaluation of a recombinant circumsporozoite protein vaccine against *Plasmodium falciparum* malaria. RTS,S Malaria Vaccine Evaluation Group. *N. Engl. J. Med.* **336**, 86–91 (1997).
11. Foquet, L. *et al.* Vaccine-induced monoclonal antibodies targeting circumsporozoite protein *prevent Plasmodium falciparum* infection. *J. Clin. Invest.* **124**, 140–144 (2014).
12. Oyen, D. *et al.* Structural basis for antibody recognition of the NANP repeats in *Plasmodium falciparum* circumsporozoite protein. *Proc. Natl. Acad. Sci. USA* **114**, E10438–E10445 (2017).
13. Olotu, A. *et al.* Four-year efficacy of RTS,S/AS01E and its interaction with malaria exposure. *N. Engl. J. Med.* **368**, 1111–1120 (2013).
14. Olotu, A. *et al.* Seven-year efficacy of RTS,S/AS01 malaria vaccine among young African children. *N. Engl. J. Med.* **374**, 2519–2529 (2016).
15. Triller, G. *et al.* Natural parasite exposure induces protective human anti-malarial antibodies. *Immunity* **47**, 1197–1209.e10 (2017).
16. Hoffman, S.L. *et al.* Development of a metabolically active, non-replicating sporozoite vaccine to prevent Plasmodium falciparum malaria. *Hum. Vaccin* **6**, 974–106 (2010).
17. Seder, R.A. *et al.* Protection against malaria by intravenous immunization with a nonreplicating sporozoite vaccine. *Science* **341**, 1359–1365 (2013).
18. Briney, B.S., Willis, J.R., Hicar, M.D., Thomas, J.W. II & Crowe, J.E. Jr. Frequency and genetic characterization of V(DD)J recombinants in the human peripheral blood antibody repertoire. *Immunology* **137**, 56–64 (2012).
19. March, S. *et al.* A microscale human liver platform that supports the hepatic stages of Plasmodium falciparum and vivax. *Cell Host Microbe* **14**, 104–115 (2013).
20. March, S. *et al.* Micropatterned coculture of primary human hepatocytes and supportive cells for the study of hepatotropic pathogens. *Nat. Protoc.* **10**, 2027–2053 (2015).
21. Espinosa, D.A. *et al.* Robust antibody and CD8$^+$ T-cell responses induced by *P. falciparum* CSP adsorbed to cationic liposomal adjuvant CAF09 confer sterilizing immunity against experimental rodent malaria infection. *NPJ. Vaccines* **2**, 10 (2017).
22. Nardin, E.H. *et al.* Circumsporozoite proteins of human malaria parasites *Plasmodium falciparum* and *Plasmodium vivax*. *J. Exp. Med.* **156**, 20–30 (1982).
23. Zavala, F. *et al.* Rationale for development of a synthetic vaccine against *Plasmodium falciparum* malaria. *Science* **228**, 1436–1440 (1985).
24. Sack, B.K. *et al.* Humoral protection against mosquito bite-transmitted *Plasmodium falciparum* infection in humanized mice. *NPJ Vaccines* **2**, 27 (2017).
25. Kublin, J.G. *et al.* Complete attenuation of genetically engineered *Plasmodium falciparum* sporozoites in human subjects. *Sci. Transl. Med.* **9**, eaad9099 (2017).
26. Vanderberg, J.P. & Frevert, U. Intravital microscopy demonstrating antibody-mediated immobilisation of *Plasmodium berghei* sporozoites injected into skin by mosquitoes. *Int. J. Parasitol.* **34**, 991–996 (2004).
27. Sack, B.K. *et al.* Model for *in vivo* assessment of humoral protection against malaria sporozoite challenge by passive transfer of monoclonal antibodies and immune serum. *Infect. Immun.* **82**, 808–817 (2014).
28. Epstein, J.E. *et al.* Safety and clinical outcome of experimental challenge of human volunteers with *Plasmodium falciparum*–infected mosquitoes: an update. *J. Infect. Dis.* **196**, 145–154 (2007).
29. Rickman, L.S. *et al. Plasmodium falciparum*–infected *Anopheles stephensi* inconsistently transmit malaria to humans. *Am. J. Trop. Med. Hyg.* **43**, 441–445 (1990).
30. Freire, E., Schön, A. & Velazquez-Campoy, A. Isothermal titration calorimetry: general formalism using binding polynomials. *Methods Enzymol.* **455**, 127–155 (2009).
31. Fisher, C.R. *et al.* T-dependent B cell responses to *Plasmodium* induce antibodies that form a high-avidity multivalent complex with the circumsporozoite protein. *PLoS Pathog.* **13**, e1006469 (2017).
32. Plassmeyer, M.L. *et al.* Structure of the *Plasmodium falciparum* circumsporozoite protein, a leading malaria vaccine candidate. *J. Biol. Chem.* **284**, 26951–26963 (2009).
33. Ghasparian, A., Moehle, K., Linden, A. & Robinson, J.A. Crystal structure of an NPNA-repeat motif from the circumsporozoite protein of the malaria parasite *Plasmodium falciparum*. *Chem. Commun. (Camb.)* **174–176**, 174–176 (2006).
34. Dyson, H.J., Satterthwait, A.C., Lerner, R.A. & Wright, P.E. Conformational preferences of synthetic peptides derived from the immunodominant site of the circumsporozoite protein of *Plasmodium falciparum* by 1H NMR. *Biochemistry* **29**, 7828–7837 (1990).
35. Topchiy, E. *et al.* T1BT* structural study of an anti-plasmodial peptide through NMR and molecular dynamics. *Malar. J.* **12**, 104 (2013).
36. Coppi, A., Pinzon-Ortiz, C., Hutter, C. & Sinnis, P. The *Plasmodium* circumsporozoite protein is proteolytically processed during cell invasion. *J. Exp. Med.* **201**, 27–33 (2005).
37. Espinosa, D.A. *et al.* Proteolytic cleavage of the *Plasmodium falciparum* circumsporozoite protein is a target of protective antibodies. *J. Infect. Dis.* **212**, 1111–1119 (2015).
38. Aurrecoechea, C. *et al.* PlasmoDB: a functional genomic database for malaria parasites. *Nucleic Acids Res.* **37**, D539–D543 (2009).
39. Rich, S.M., Hudson, R.R. & Ayala, F.J. *Plasmodium falciparum* antigenic diversity: evidence of clonal population structure. *Proc. Natl. Acad. Sci. USA* **94**, 13040–13045 (1997).
40. Zeeshan, M. *et al.* Genetic variation in the *Plasmodium falciparum* circumsporozoite protein in India and its relevance to RTS,S malaria vaccine. *PLoS One* **7**, e43430 (2012).
41. Zakeri, S., Avazalipoor, M., Mehrizi, A.A., Djadid, N.D. & Snounou, G. Restricted T-cell epitope diversity in the circumsporozoite protein from *Plasmodium falciparum* populations prevalent in Iran. *Am. J. Trop. Med. Hyg.* **76**, 1046–1051 (2007).
42. Tanabe, K. *et al.* Within-population genetic diversity of *Plasmodium falciparum* vaccine candidate antigens reveals geographic distance from a Central sub-Saharan African origin. *Vaccine* **31**, 1334–1339 (2013).
43. Gaudinski, M.R. *et al.* Safety and pharmacokinetics of the Fc-modified HIV-1 human monoclonal antibody VRC01LS: a phase 1 open-label clinical trial in healthy adults. *PLoS Med.* **15**, e1002493 (2018).
44. Wu, X. *et al.* Rational design of envelope identifies broadly neutralizing human monoclonal antibodies to HIV-1. *Science* **329**, 856–861 (2010).

ONLINE METHODS

Study subjects and clinical specimens. Sera from protected volunteers in the VRC 312 clinical trial (https://clinicaltrials.gov/; NCT01441167) were screened for the titer of PfCSP-specific antibodies and for inhibition of sporozoite invasion of hepatocytes *in vitro*[16,17]. Briefly, this was a phase 1, open-label, dose-escalation study investigating safety, immunogenicity and protective efficacy of the Sanaria PfSPZ Vaccine made from radiation-attenuated aseptic, purified, cryopreserved PfSPZ of the NF54 strain. Memory B cell–derived monoclonal antibodies against PfCSP were isolated from peripheral blood mononuclear cells (PBMCs) taken 2 weeks after the last vaccine dose in a protected donor who received five doses of 1.35×10^5 PfSPZs. Plasmablast PfCSP-specific monoclonal antibodies were isolated from two volunteers in the VRC 314 clinical trial (https://clinicaltrials.gov/; NCT02015091)[45,46]. These subjects received a total of four doses of the PfSPZ Vaccine intravenously at week 0, 4, 12 and 20 (the first two doses were 2.7×10^5 PfSPZs and the following two doses were 4.5×10^5 PfSPZs). Plasmablasts were isolated from PBMCs at 7 d after the third immunization.

Ethics statement for mouse studies. All mouse research complied with the Institutional Animal Care and Use Committee (IACUC) of Johns Hopkins University (Approved protocol permit no. MO16H35) and was performed in accordance with protocols approved by the Center for Infectious Disease Research IACUC; (protocol no. SK-16). The Seattle Biomed IACUC adheres to the National Institutes of Health Office of Laboratory Animal Welfare standards (OLAW; welfare assurance no. A3640-01).

rPfCSP probes generation. The amino acid sequence of PfCSP of 3D7 (PlasmoDB ID: PF3D7_0304600.1), a clone of the NF54 strain, was used to generate a codon-optimized synthetic gene for expression in mammalian cells (GenScript). The DNA construct corresponding to the full-length rPfCSP, in which the leader peptide residues 1–20 were replaced with a mammalian secretory signal peptide derived from the modified bovine prolactin (MDSKGSSQ KGSRLLLLLVVSNLLLPQGVLA) and the glycosylphosphatidylinositol (GPI) anchor residues 376–397 were excluded, was cloned into a CMV/R-expression vector with C-terminal AviTag, HRV3C-processing tag and a histidine tag[44,47,48]. This construct encodes the native N-terminal domain, the central domain consisting of $(NANP)_{38}$ tandem repeats with four interspersed NVDP, and the C-terminal domain. PfCSP mutants were generated through site-directed mutagenesis (GenScript). rPfCSP or PfCSP mutants were expressed through transient transfection in Expi293 cells (Life Technologies) according to the manufacturer's instructions and were purified from culture supernatants through polyhistidine-tag affinity chromatography (GE Healthcare) followed by gel filtration. Fractions containing monomers were pooled, concentrated and frozen at −80 °C. For tetramer probe generation, the repeat peptide $(NANP)_9$ or rPfCSP were first biotinylated and then conjugated to fluorophore. rPfCSP was biotinylated using ligase Bir A (Avidity) at 30 °C for 4 h and was buffer exchanged with PBS (pH 7.4) over a 30-kDa Centricon Plus-70 Centrifugal Filter (Millipore) to remove excess free biotin. The repeat peptide $(NANP)_9$ was synthetically made and biotinylated at its N terminus through the lysine analog Ahx linker (GenScript). Biotinylated rPfCSP and $(NANP)_9$ peptide were fluorescently labeled through sequential addition of streptavidin conjugated to allophycocyanin (SA-APC) or phycoerythrin (SA-PE) (Life Technologies) in a 4:1 molar ratio[44].

Isolation of PfCSP-specific memory B cells. PBMCs (10^6) were stained with the following panel: Aqua LIVE/DEAD (Invitrogen, cat. no. L34966), the tetramer probes rPfCSP-APC and $(NANP)_9$-PE generated as described above, and antibodies against CD3-BV510 (BioLegend, cat. no. 317332), CD8-BV510 (BioLegend, cat. no. 311040), CD14-BV510 (BioLegend, cat. no. 301842), CD56-BV510 (BioLegend, cat. no. 318340), CD19-ECD (Beckman Coulter, cat. no. IM2708U), CD27-QD605 (Invitrogen cat. no. Q10065), CD21-Cy5PE (BD Biosciences, cat. no. 551064), CD38–Alexa Fluor 680 (BD Biosciences, cat. no. 560676), IgD Cy7PE (BD Biosciences, cat. no. 561314), IgM Cy5.5-PerCP (BD Biosciences, cat. no. 561285) and IgG Cy7PE (BD Biosciences cat. no. 561298). Cells were acquired and sorted using a BD FACS Aria II instrument (BD Immunocytometry Systems), and fluorescence-activated cell sorting (FACS) data was analyzed using FlowJo software (Tree Star). The gating strategy is shown in **Figure 1a**. PfCSP-reactive (rPfCSP$^+$ and/or $(NANP)_9^+$) CD19$^+$CD27$^+$IgG$^+$IgD$^-$IgM$^-$ memory B cells were single-cell dry-sorted into 96-well PCR plates, rapidly frozen on dry ice and stored at −80 °C until processing[44,47].

Isolation of plasmablasts. PBMCs were freshly isolated from blood samples collected 7 d after PfSPZ immunization and stained for viability with Aqua LIVE/DEAD dye (Invitrogen, Cat. No. L34966) followed by surface staining for the following markers: CD20-Cy7APC (BD Bioscience, cat. no. 335794), CD19-FITC (BD Bioscience, cat. no. 555412), CD3-Cy7PE (BD Bioscience, cat. no. 557851), CD38-PE (BD Bioscience, cat. no. 555460) and CD27-APC (ThermoFisher, cat. no. 17-0279-42). Plasmablasts were gated as live, CD3$^-$CD20$^-$CD19$^+$CD27$^+$CD38$^+$ and were sorted as single cells into 96-well PCR plates containing 20 µl/well of reverse transcriptase reaction buffer that included 5 µl of 5× first-strand cDNA buffer, 0.5 µl of RNAseOut (Invitrogen), 1.25 µl of dithiothreitol (DTT), 0.0625 µl of igepal and 13.25 µl of distilled H_2O (Invitrogen) as previously described[49].

Production of recombinant immunoglobulins. Following a single sorting of rPfCSP-specific memory B cells, lysis buffer was added to the plate, and the genes encoding the variable region of the heavy and light chains of IgG were amplified through RT-PCR and re-expressed as described previously[50]. Briefly, amplification of rearranged genes encoding the variable regions of IgG heavy, kappa or lambda chains was performed using a cocktail of primers followed by sequencing and cloning into expression vectors containing the relevant constant region. Matched heavy and light chain constructs derived from each sorted cell were coexpressed using Expi293 cells, and 28 full-length IgG were purified using a recombinant protein-A column (GE Healthcare). Sequence analysis was performed using IMGT, the international immunogenetics information system (http://www.imgt.org/)[51].

Similarly, immunoglobulin-encoding genes of plasmablasts were amplified through RT and nested PCR without cloning from RNA of single sorted cells as previously described[49,52]. The amplified rearranged gene segments encoding variable regions were assembled into the corresponding linear full-length immunoglobulin heavy- and light-chain gene expression cassettes through PCR as previously described[49,52]. Heavy and light chain linear cassettes were cotransfected in 293T cells using Effectene with enhancer (Qiagen)[49,52]. Transfected cultures were incubated at 37 °C 5% CO_2 for 3 d. Supernatants were harvested, concentrated and purified using HiTrap Protein A prepacked high-performance plates (GE Healthcare) for 20 min at room temperature on a shaker. Following wash with PBS and NaCl, eluates were neutralized with Trizma hydrochloride and buffer exchanged with PBS before determining antibody concentration using Nanodrop.

ELISA. MaxiSorp ELISA plates (Thermo Scientific Nunc) were coated with 100 µl of rPfCSP (1 µg/ml) per well for 1 h at room temperature according to the manufacturer's instructions (KPL). Coated plates were blocked with 100 µl of 1× blocking solution for 1 h at room temperature, which was followed by incubation with 100 µl of PfCSP monoclonal antibodies, mock transfection filtrate or control antibodies (VRC 01, a human anti-HIV-1 IgG1 as an isotype-matched negative control[44]; 2A10, a mouse monoclonal antibody specific for the NANP-repeat region of PfCSP[20,21]) at varying concentrations (0.00006–5.0 µg/ml). After 1 h, plates were incubated with 100 µl/well of 1.0 µg/ml peroxidase-labeled goat anti–human IgG antibody (KPL, cat. no. 04-10-06). Plates were washed six times with PBS-Tween between each step. After a final wash, samples were incubated for about 15 min with the ABTS peroxidase (KPL, cat. no. 50-62-10) or Ultra TMB ELISA (Invitrogen, cat. no. 34029) substrate. The optical density was read at 405 or 450 nm after addition of stopping solution (100 µl/well).

For the PfSPZ ELISA, serially diluted (0.06–1.0 µg/ml) PfCSP-specific monoclonal antibodies or indicated controls were added to the PfSPZ-coated plates and incubated for 1 h. ELISA was then performed as described above.

Epitope mapping of PfCSP monoclonal antibodies. Mapping of the PfCSP-specific monoclonal antibody epitopes was performed as previously described[53] using linear PfCSP peptides that were 15 amino acids in length (GenScript) and that overlapped by 11 residues spanning the full length of PfCSP. MaxiSorp

ELISA plates (Thermo Scientific Nunc) were coated with 100 µl of peptides (10 µg/ml). Following overnight incubation, plates were blocked with PBS + 0.05% Tween-20 and 1% BSA (Sigma-Aldrich) for 1 h. Plates were incubated with 100 µl of PfCSP-specific monoclonal antibodies or controls at varying concentrations (0.00006–5.0 µg/ml). After 1 h, plates were incubated with 100 µl/well of peroxidase-labeled goat anti-human (Invitrogen, cat. no. A18811) or rabbit anti-mouse (Thermo Fisher Scientific, cat. no. 61-6520) secondary antibody, at a 1:20,000 dilution in PBST-1% BSA. All the incubation steps were done at room temperature. Plates were washed six times with PBS-Tween between each step. After a final wash, samples were incubated for about 15 min with the TMB Plus Reagent (Thermo Fisher Scientific) according to the manufacturer's instructions. The optical density was read at 450 nm after addition of stopping solution (100 µl/well).

Competitive ELISA was performed as previously reported[37] using selected peptides. Briefly, ELISA plates were coated with 100 µl of rPfCSP (200 ng/ml) overnight. After blocking plates with PBS with 1% BSA for 1 h, PfCSP-specific monoclonal antibodies (10 ng/ml) preincubated overnight with varying concentrations (0–1,000 µg/ml) of selected PfCSP peptides in PBS with 1% BSA were added to the rPfCSP-coated plates, and we performed ELISA as described above. For the alanine scanning mutagenesis experiments, competitive ELISA was performed as described above using peptide 21 variants (GenScript).

To determine the inhibitory effect of PfCSP peptides on binding of CIS43 to PfSPZ, MaxiSorp ELISA plates (Thermo Scientific Nunc-Immuno) precoated with 5×10^3 PfSPZs were blocked with PBS with 2% BSA (Sigma) for 1 h at room temperature and were washed with PBS before addition of CIS43 (10 ng/ml). The mixture was preincubated overnight with varying concentrations (0–1,000 µg/ml) of the PfCSP peptides, and then an ELISA was performed as described above.

Indirect fluorescence assay. Freshly isolated PfSPZs (3×10^3) were air-dried on poly-L-lysine-coverslips (Tekdon Inc.) and incubated for 30 min at room temperature with varying concentrations (0.0002–1.0 µg/ml) of PfCSP-specific monoclonal antibodies or control antibodies. After washing with PBS with 1% BSA, slides were incubated with FITC-labeled goat anti-Human IgG (Fcγ) (Jackson ImmunoResearch, cat. no. 109-095-008), and green fluorescent sporozoites were visualized using an upright Nikon Eclipse 90i fluorescence microscope[37].

Kinetic binding assay using biolayer interferometry. Antibody binding kinetics were measured using biolayer interferometry on an Octet Red384 instrument (fortéBio) using streptavidin-capture biosensors (fortéBio). PfCSP monoclonal antibody solutions were plated in solid black tilt-well 96-well plates (Geiger Bio-One); assays were performed with agitation at 30 °C. Loading of biotinylated rPfCSP or peptides 21 and 29 was performed for 300 s, followed by dipping the biosensors into buffer (PBS + 1% BSA) for 60 s to assess baseline assay drift. Association with whole IgG (serially diluted from 267 to 33 µM) was done for 300 s, followed by a dissociation step in buffer for 600 s. Background subtraction of nonspecific binding was performed through measurement of association in buffer alone. Data analysis and curve fitting were performed using Octet software, version 7.0. Experimental data were fitted with the binding equations describing a 1:1 heterologous ligand interaction. Global analyses of the complete data sets, assuming binding was reversible (full dissociation), were carried out using nonlinear least-squares fitting allowing a single set of binding parameters to be obtained simultaneously for all concentrations of a given monoclonal antibody dilution series.

***In vitro* functional inhibition assay of PfSPZ invasion of hepatocytes.** Micropatterned coculture (MPCC) preparation and Pf infection were carried out as described previously[17,18]. Briefly, glass-bottom 96-well plates were coated homogenously with rat tail type I collagen (50 µg/ml) and subjected to soft-lithographic techniques to pattern the collagen into microdomains of 500-µm islands that mediate selective hepatocyte adhesion. To create MPCCs, cryopreserved primary human hepatocytes (BioreclamationIVT) were pelleted through centrifugation at 100*g* for 6 min at 4 °C, assessed for viability using trypan blue exclusion (typically, 70–90% excluded the dye) and seeded on collagen-micropatterned plates. Each well contained approximately 10,000 hepatocytes organized in colonies of 500 µm in serum-free DMEM with 1% PenStrep. 2–3 h later, cells were washed with serum-free DMEM with 1% PenStrep, and the medium was switched to human hepatocyte culture medium. 1 d after seeding, PfCSP-specific monoclonal antibodies were added in triplicate at four concentrations (10, 1.0, 0.1 and 0.01 µg/ml) to the MPCCs, 30–45 min before infection with 7.5×10^4 fresh PfSPZs per well. After 3 h, cultures were washed with hepatocyte culture medium with 3% PenStrep and 0.1% Fungizone, and 7,000 3T3-J2 fibroblasts were added to create the coculture. Medium was replaced daily. Samples were fixed on day 3.5 post infection. The impact of the antibodies on hepatocyte infection was assessed through calculating the number of liver-stage parasites or exoerythrocytic forms (EEFs) present at day 3.5 of infection. EEFs were determined through staining for PfHSP70 and visualized with a Nikon Eclipse Ti fluorescence microscope.

***In vivo* protection in C57BL/6 mice with chimeric Pb-PfCSP SPZ.** For i.v. challenge, 6- to 8-week-old C57BL/6 mice (5mice per group) were i.v. injected with control antibodies or varying concentrations of PfCSP-specific monoclonal antibodies diluted in PBS (pH 7.4) for a total volume of 200 µl per mouse and immediately challenged with 2,000 Pb chimeric SPZ–expressing PfCSP (Pb-PfCSP SPZ). Forty hours later, livers were excised and RNA was isolated for quantification of the Pb-specific 18s rRNA levels through RT-qPCR[54,55].

For the mosquito bite challenge, female *Anopheles stephensi* mosquitoes were allowed to feed on 8-week-old Swiss webster mice infected with blood-stage Pb-PfCSP. The proportion of infected mosquitoes was then determined by salivary gland dissection 18 d after the blood meal, and this value was used to calculate the number of mosquitoes needed to challenge mice with the equivalent of ~5 infected mosquitoes per mouse. As an example, if 9 out of 12 (75%) mosquitoes were infected, then 6 or 7 mosquitoes were needed per mouse. Mosquito infection rates ranged 75–90%. C57BL/6 mice (up to 7 per group) were i.v. injected with various concentrations (30–300 µg) of PfCSP-specific monoclonal antibodies as described above. Ten minutes later, mice were anesthetized with 2% avertin (Alfa Aesar), and the infected mosquitoes were allowed to feed on mice for ~10 min, after which mosquito abdomens were visually inspected for blood, indicating the mosquito has bitten. Mouse parasitemia was assessed daily through Giemsa staining of blood smears from day 4 through day 12 postinfection.

***In vivo* protection in FRG-huHep mice.** Passive transfer of control antibodies and PfCSP-specific monoclonal antibodies, and infectious challenge in FRG-huHep mice was done as previously described[27]. Briefly, FRG-huHep mice, purchased from Yecuris, Inc., were given 30–150 µg of PfCSP-specific monoclonal antibodies or controls intraperitoneally (i.p.) 16–24 h before infection. Fifty *Anopheles* mosquitos infected with Pf that expressed GFP-luciferase[56] were allowed to feed for 10 min on FRG-huHep mice. Six days postchallenge, mice were imaged following i.p. administration of 100 µl of Rediject D-luciferin (PerkinElmer) using bioluminescence and IVIS imaging to determine the liver-stage parasite burden as previously described[27,57]. Total flux (pixels/second) was measured after choosing an equivalent region of interest around each mouse liver. Liver-stage parasite burden was normalized using the average of the negative control group that received the isotype species-matched IgG.

For sterile protection, FRG-huHep mice were i.p. injected with control antibodies or PfCSP-specific monoclonal antibodies (50 µg per mouse) as described above. The following day, mice were challenged with the bites of 5 Pf-infected mosquitoes per mouse. At approximately day 6.5, all mice were injected with 400 µl of packed human red blood cells at 70% hematocrit in RPMI. On day 7 and day 9, mice were bled via the retroorbital plexus, and 50 µl was mixed into 1 ml of NucliSens EasyMag buffer (BioMerieux) and placed at –80 °C until extraction. Total RNA extraction and qPCR to determine the number of Pf 18s rRNA copies was performed as previously described[58]. Mice were considered positive if any parasite RNA the above background level (reaction with no nucleic acid) was detected in blood.

ELISA for quantitation of monoclonal antibody concentration in serum. To assess circulating levels of passively transferred PfCSP-specific monoclonal antibodies, FRG-huHep mice were bled via the retroorbital plexus immediately before challenge with infectious mosquito bites. ELISA was performed on mouse serum as previously described using of rPfCSP-coated plates (2 µg/ml). A standard curve for each monoclonal antibody was generated using eight

doi:10.1038/nm.4512

twofold dilutions of monoclonal antibody starting at 625 ng/ml. Serum samples were applied at a 1:160 and 1:320 dilution in dilution/blocking buffer. The average of the 1:160 and 1:320 calculated concentration values was used for each individual sample.

Antigen-binding fragment expression and purification. Genes encoding antibody heavy and light chains were cotransfected into GnTI- cells (ATCC). Six days following transfection, supernatant was harvested, and antibodies were purified over a protein A resin column, washed with five column volumes of PBS and eluted with IgG Elution buffer (Pierce). Tris (1 M) was added immediately to neutralize the pH to ~7.4. IgGs were then digested with Lys C overnight at 37 °C (1 µg for 10 mg of IgG), and the antigen-binding fragments were purified further through collecting the flowthrough of Protein A column and through size-exclusion chromatography in 5 mM Hepes, 150 mM NaCl. For antigen-binding fragment–peptide preparations, peptides were dissolved in DMSO and added to the antigen-binding fragments at a 50% molar excess.

Isothermal titration calorimetry. Isothermal titration calorimetry (ITC) was carried out using VP-ITC microcalorimeters from MicroCal/Malvern Instruments. In all titration experiments, rPfCSP, PfCSP mutants and PfCSP-specific monoclonal antibodies (whole IgG or antigen-binding fragments) were prepared in PBS, pH 7.4. Each antibody solution, prepared at a concentration of ~100 µM (expressed per antigen-binding fragment site), was injected in 10-µl aliquots into the calorimetric cell containing rPfCSP at a concentration of ~1 µM. Peptides 21 or 29 and CIS43 were prepared in PBS, pH 7.4, with 2% DMSO. The CIS43 solution, prepared at a concentration of 50 µM (expressed per antigen-binding fragment site), was injected in 10-µl aliquots into the calorimetric cell containing the peptide at a concentration of 2 µM. All titrations were performed at 25 °C. Except for the concentration of the peptides, which was based on weight, the exact concentrations of the reactants in each experiment were determined from the protein absorbance at 280 nm. The heat evolved upon each injection of antibody was obtained from the integral of the calorimetric signal. The heat associated with binding of the antibody to rPfCSP or the peptide in the cell was obtained through subtracting the heat of dilution from the heat of reaction. The enthalpy change (ΔH), the association constant (K_a), the dissociation constant, ($K_d = 1 / K_a$) and the stoichiometry (N) were obtained through nonlinear regression of the individual heats as a function of the concentrations to fit a model that takes into account the binding to two sets of sites with different binding energetics for rPfCSP or to a single-binding-site model for the peptides. The change in Gibbs energy (ΔG), was calculated from the relation $\Delta G = -RT\ln K_a$, where R is the is the universal gas constant (1.987 cal/(K × mol)) and T is the absolute temperature in kelvin. The entropy contribution to Gibbs energy, $-T \times \Delta S$, was calculated from the known relation $\Delta G = \Delta H - (T \times \Delta S)$.

Crystallization and data collection. The crystal structures of the CIS43 antigen-binding fragment bound to PfCSP peptides 20, 21, 25 or 29 were obtained using a mosquito (ttplabtech) and NT8 (Formulatrix)-dispensing robots. Screening was done with Rigaku Wizard Precipitant Synergy block no. 2, Molecular Dimensions Proplex screen HT-96 and Hampton Research Crystal Screen HT using the vapor diffusion method. Crystals used for diffraction data were grown in the following conditions: CIS43 antigen-binding fragment with peptide 20: 0.2M Ammonium Sulfate, 0.1M sodium acetate trihydrate pH 4.6, 30% PEG MME 2000; CIS43 antigen-binding fragment with peptide 21: 0.1M sodium acetate trihydrate pH 4.6, 2 M ammonium sulfate; CIS43 antigen-binding fragment with peptide 25: 0.1 M HEPES sodium pH 7.5, 1.4 M sodium citrate tribasic dihydate; CIS43 antigen-binding fragment with peptide 29: 1.6 M sodium citrate tribasic dihydrate pH 6.5, using the vapor diffusion method. Crystals were cryoprotected in solutions containing 30% molar excess of their original reagents and 20% ethylene glycol. Crystals diffracted to 2.4 Å, 1.8 Å, 2.0 Å and 2.2 Å (**Supplementary Table 3**).

The crystal structure of the CIS42 antigen-binding fragment bound to peptide 20, 21, 25 or 29 was obtained following the same procedure as described above. Crystals used for diffraction data were all grown in 15% PEG3350, 9% isopropanol, 0.12 M ammonium citrate pH 8.5. Crystals were cryoprotected in solutions containing 30% molar excess of their original reagents and 20% ethylene glycol. Crystals of the CIS42 antigen-binding fragment with peptide 20, peptide 21, peptide 25 and peptide 29 diffracted to 2.3 Å, 1.8 Å, 2.0 Å and 2.2 Å, respectively (**Supplementary Table 5**). Data were collected at ALS 5.01, 5.02 and on the Fred Hutchinson Cancer Research Center home source (Rigaku) and processed using HKL2000 (ref. 59).

Structure solution and refinement. The structures of the CIS43 antigen-binding fragment and the CIS42 antigen-binding fragment with peptides were solved through molecular replacement using Phaser in CCP4 (ref. 60). The peptides were manually fitted using COOT[61], and refinement of the structures was done in Phenix[62]. The refinement statistics are summarized in **Supplementary Tables 3** and **5**. Structural figures were made with Pymol (https://ci.nii.ac.jp/naid/10026107904/).

Molecular dynamic simulations. Four protein systems were created based on the crystal structures: the CIS43 antigen-binding fragment in complex with peptide 21, the CIS42 antigen-binding fragment in complex with peptide 21, free peptide 21 in its conformation when bound to the CIS43 antigen-binding fragment, and free peptide 21 in its conformation when bound to the CIS42 antigen-binding fragment. All protein models were immersed in a water box neutralized to 0.15 M with sodium chloride ions. The water box was built using the Solvate plugin, and the ions were added with the Autoionize plugin (Visual Molecular Dynamics)[63]. Protein structure files were created using the psfgen function (Visual Molecular Dynamics).

The four protein systems were then configured to run with NAMD2.12 (Scalable Molecular Dynamics)[64] with the CHARMM36 force field[65]. TIP3P water parameterization was used to describe the water molecules. All systems were fully minimized with 20,000 conjugate gradient steps before proceeding with equilibration runs. Equilibration began with a slow heating starting at 100 K until reaching a final temperature of 310 K. Simulations were performed with a 1-fs timestep for all equilibration and production runs. The periodic electrostatic interactions were computed using particle-mesh Ewald (PME) summation with a grid spacing <1 Å. A constant temperature was imposed by using Langevin dynamics with a damping coefficient of 1.0 ps. A constant pressure of 1 atm was maintained with Langevin piston dynamics, a 200-fs decay period and a 50-fs time constant.500 ns of molecular dynamics simulation on the National Institutes of Health High-Performance Computing Cluster (https://hpc.nih.gov/) was achieved for all four protein systems.

Peptide 21 was assessed with root mean square deviation (RMSD) and root mean square fluctuation (RMSF). RMSD was calculated using VMD's Trajectory Tool plugin, and RMSF was calculated with Gromacs[66]. Both were calculated over the full 500-ns trajectory, and results were compared side-by-side. For RMSD and RMSF, the antibodies were aligned to frame 1 of the respective trajectories in order to compare conformation changes and movement of peptide 21. Additionally, principal component analysis (PCA) was performed using mdtraj[67] and scikit[68] and was graphed with matplotlib[69] to visualize the distribution of structural conformations of free peptide 21. Peptide 21 in its conformations bound to the CIS43 antigen-binding fragment and the CIS42 antigen-binding fragment were plotted on the PCA density heatmap. Eigenvalues are listed to show principal component 1 and principal component 2 as the dominant components. Hydrogen bond analysis was performed with UCSF Chimera[70] on peptide 21 for both the CIS43 antigen-binding fragment and CIS42 antigen-binding fragment simulations, and the number of hydrogen bonds are shown over the 500-ns trajectory. Lastly, the crystal structures of the CIS43 antigen-binding fragment and the CIS42 antigen-binding fragment were aligned to their 500-ns frames, and RMSD was calculated to compare movement and flexibility of the antibody complementarity-determining region loops. Using the CIS43 antigen-binding fragment bound to peptide 21 as input, free energy calculations of mutant and wild-type CIS43 were performed computationally using FoldX. The protein structure was repaired, mutated, and binding energy was calculated[71].

Pulse-chase metabolic labeling assay. Pulse-chase metabolic labeling of *Plasmodium* sporozoites has been previously described[36,37]. Briefly, freshly dissected Pf sporozoites were incubated in DMEM without Cys and Met, 1% BSA and 400 µCi/ml L-[^{35}S]-Cys and L-[^{35}S]-Met for 45 min at 28 °C and then kept on ice or chased at 28 °C for 1.5 h in DMEM with Cys and Met and 1% BSA in the absence or presence of the indicated concentrations of antibodies: mAb15

(negative control, human monoclonal antibody specific for the C terminus of PfCSP; **Supplementary Fig. 1c**), 5D5 (positive control, mouse monoclonal antibody specific for the N terminus of PfCSP)[37] and CIS43 monoclonal antibody. Following the lysis of chased sporozoites, labeled PfCSP was immunoprecipitated with 2A10 (mouse monoclonal antibody specific for PfCSP repeats)[21,22] conjugated to sepharose. Labeled PfCSP was eluted from the beads and analyzed using SDS-PAGE and autoradiography. Densitometry of the high- and low-molecular-weight bands was performed using ImageJ software. The ratio of the density, or area under the curve, of the top band to that of the bottom band was calculated.

Statistics. For liver-stage parasite burden in C57BL/6 mice, data were compared for significance using a Mann–Whitney test, whereas in FRG-huHep mice, the Kruskal–Wallis test with Dunn's correction for multiple comparisons was used. Kaplan–Meier curves for parasitemia were analyzed using the log-rank test. For measurement of PfCSP-specific monoclonal antibodies in mouse serum, standard curves were fitted with a hyperbolic parameter curve, and concentration values were interpolated. For the stoichiometry data, errors with 95% confidence were estimated from the fits of the data. Unless otherwise indicated, all data were plotted and graphed using GraphPad Prism, version 7.0. $P < 0.05$ indicated a statistically significant difference.

Life Sciences Reporting Summary. Further information on experimental design and reagents is available in the **Life Sciences Reporting Summary**.

Data availability. The authors declare that all the data supporting the findings of this study are available within the paper and supplementary information files. The structure factors and coordinates of CIS43 and CIS42 bound to peptide 20, 21, 25 and 29 have been deposited in the Protein Data Bank (PDB) with accession codes 6B5L, 6B5M, 6B5N, 6B5O, 6B5P, 6B5R, 6B5S and 6B5T, respectively.

45. Ishizuka, A.S. *et al.* Protection against malaria at 1 year and immune correlates following PfSPZ vaccination. *Nat. Med.* **22**, 614–623 (2016).
46. Lyke, K.E. *et al.* Attenuated PfSPZ Vaccine induces strain-transcending T cells and durable protection against heterologous controlled human malaria infection. *Proc. Natl. Acad. Sci. USA* **114**, 2711–2716 (2017).
47. Wheatley, A.K. *et al.* H5N1 vaccine–elicited memory B cells are genetically constrained by the IGHV locus in the recognition of a neutralizing epitope in the hemagglutinin stem. *J. Immunol.* **195**, 602–610 (2015).
48. Kanekiyo, M. *et al.* Rational design of an Epstein–Barr virus vaccine targeting the receptor-binding site. *Cell* **162**, 1090–1100 (2015).
49. Liao, H.X. *et al.* High-throughput isolation of immunoglobulin genes from single human B cells and expression as monoclonal antibodies. *J. Virol. Methods* **158**, 171–179 (2009).
50. Tiller, T. *et al.* Efficient generation of monoclonal antibodies from single human B cells by single cell RT-PCR and expression vector cloning. *J. Immunol. Methods* **329**, 112–124 (2008).
51. Lefranc, M.P. *et al.* IMGT, the international immunogenetics information system. *Nucleic Acids Res.* **37**, D1006–D1012 (2009).
52. Bonsignori, M. *et al.* Analysis of a clonal lineage of HIV-1 envelope V2/V3 conformational epitope-specific broadly neutralizing antibodies and their inferred unmutated common ancestors. *J. Virol.* **85**, 9998–10009 (2011).
53. Douglas, A.D. *et al.* Neutralization of *Plasmodium falciparum* merozoites by antibodies against PfRH5. *J. Immunol.* **192**, 245–258 (2014).
54. Chomczynski, P. & Sacchi, N. Single-step method of RNA isolation by acid guanidinium thiocyanate-phenol-chloroform extraction. *Anal. Biochem.* **162**, 156–159 (1987).
55. Bruña-Romero, O. *et al.* Detection of malaria liver-stages in mice infected through the bite of a single *Anopheles* mosquito using a highly sensitive real-time PCR. *Int. J. Parasitol.* **31**, 1499–1502 (2001).
56. Vaughan, A.M. *et al.* A transgenic *Plasmodium falciparum* NF54 strain that expresses GFP-luciferase throughout the parasite life cycle. *Mol. Biochem. Parasitol.* **186**, 143–147 (2012).
57. Miller, J.L. *et al.* Quantitative bioluminescent imaging of pre-erythrocytic malaria parasite infection using luciferase-expressing *Plasmodium yoelii*. *PLoS One* **8**, e60820 (2013).
58. Murphy, S.C. *et al.* Real-time quantitative reverse transcription PCR for monitoring of blood-stage *Plasmodium falciparum* infections in malaria human challenge trials. *Am. J. Trop. Med. Hyg.* **86**, 383–394 (2012).
59. Otwinowski, Z. & Minor, W. Processing of X-ray diffraction data collected in oscillation mode. *Methods Enzymol.* **276**, 307–326 (1997).
60. Collaborative Computational Project, Number 4. The CCP4 suite: programs for protein crystallography. *Acta Crystallogr. D Biol. Crystallogr.* **50**, 760–763 (1994).
61. Emsley, P. & Cowtan, K. Coot: model-building tools for molecular graphics. *Acta Crystallogr. D Biol. Crystallogr.* **60**, 2126–2132 (2004).
62. Adams, P.D. *et al.* PHENIX: a comprehensive Python-based system for macromolecular structure solution. *Acta Crystallogr. D Biol. Crystallogr.* **66**, 213–221 (2010).
63. Humphrey, W., Dalke, A. & Schulten, K. VMD: visual molecular dynamics. *J. Mol. Graph* **14**, 33–38, 27–28 (1996).
64. Phillips, J.C. *et al.* Scalable molecular dynamics with NAMD. *J. Comput. Chem.* **26**, 1781–1802 (2005).
65. Huang, J. & MacKerell, A.D. Jr. CHARMM36 all-atom additive protein force field: validation based on comparison to NMR data. *J Comput. Chem.* **34**, 2135–2145 (2013).
66. Páll, S. *et al.* Tackling exascale software challenges in molecular dynamics simulations with GROMACS. In *Solving Software Challenges for Exascale* (eds. Markadis, S. & Laure, E.) 3–27 (Springer, Cham, 2015).
67. McGibbon, R.T. *et al.* MDTraj: a modern open library for the analysis of molecular dynamics trajectories. *Biophys. J.* **109**, 1528–1532 (2015).
68. Pedregosa, F. *et al.* Scikit-learn: machine learning in Python. *J. Mach. Learn. Res.* **12**, 2825–2830 (2011).
69. Hunter, J.D. Matplotlib: a 2D graphics environment. *Comput. Sci. Eng.* **9**, 90–95 (2007).
70. Pettersen, E.F. *et al.* UCSF Chimera—a visualization system for exploratory research and analysis. *J. Comput. Chem.* **25**, 1605–1612 (2004).
71. Guerois, R., Nielsen, J.E. & Serrano, L. Predicting changes in the stability of proteins and protein complexes: a study of more than 1000 mutations. *J. Mol. Biol.* **320**, 369–387 (2002).

doi:10.1038/nm.4512

nature research

Corresponding author(s): Robert A. Seder

Life Sciences Reporting Summary

Nature Research wishes to improve the reproducibility of the work that we publish. This form is intended for publication with all accepted life science papers and provides structure for consistency and transparency in reporting. Every life science submission will use this form; some list items might not apply to an individual manuscript, but all fields must be completed for clarity.

For further information on the points included in this form, see Reporting Life Sciences Research. For further information on Nature Research policies, including our data availability policy, see Authors & Referees and the Editorial Policy Checklist.

Please do not complete any field with "not applicable" or n/a. Refer to the help text for what text to use if an item is not relevant to your study.
For final submission: please carefully check your responses for accuracy; you will not be able to make changes later.

Experimental design

1. Sample size

Describe how sample size was determined.

For the in vivo liver burden and protection experiments, the size of the experimental and control groups to detect statistical differences was based on the estimates of anticipated variation of rodent models of malaria infection and on statistical analysis from prior studies with the same experimental models. The effect of each monoclonal antibody was compared to naïve controls in assessing reduction in liver load following IV sporozoite infection, and determining protection by blood smear using a mosquito challenge. Five mice per control and experimental groups will be sufficient to show statistical differences between groups using type I and type II error rates of 0.05 and 0.10, respectively. These experiments were repeated several times for independent confirmation of the findings.

2. Data exclusions

Describe any data exclusions.

No data has been excluded

3. Replication

Describe the measures taken to verify the reproducibility of the experimental findings.

All analysis for antibody binding, specificity and functional inhibition in vitro and in vivo have been performed at least twice. Many of these analysis including in vivo protection studies have been repeated several additional times with similar results. All of the data in which we could perform statistical analysis showed that the differences observed were significant and highly consistent from experiment to experiment. Moreover, we used different assays to substantiate the major findings of the study.

4. Randomization

Describe how samples/organisms/participants were allocated into experimental groups.

Age matched litter mates were used in the different experimental groups.

5. Blinding

Describe whether the investigators were blinded to group allocation during data collection and/or analysis.

All of the functional in vitro and in vivo assays were done in a blinded manner so our collaborators who performed these analysis did not know the specifics of the antibodies tested.

Note: all in vivo studies must report how sample size was determined and whether blinding and randomization were used.

Nature Medicine: doi:10.1038/nm.4512

6. Statistical parameters

For all figures and tables that use statistical methods, confirm that the following items are present in relevant figure legends (or in the Methods section if additional space is needed).

n/a	Confirmed
☐	☒ The exact sample size (*n*) for each experimental group/condition, given as a discrete number and unit of measurement (animals, litters, cultures, etc.)
☐	☒ A description of how samples were collected, noting whether measurements were taken from distinct samples or whether the same sample was measured repeatedly
☐	☒ A statement indicating how many times each experiment was replicated
☐	☒ The statistical test(s) used and whether they are one- or two-sided *Only common tests should be described solely by name; describe more complex techniques in the Methods section.*
☐	☒ A description of any assumptions or corrections, such as an adjustment for multiple comparisons
☐	☒ Test values indicating whether an effect is present *Provide confidence intervals or give results of significance tests (e.g. P values) as exact values whenever appropriate and with effect sizes noted.*
☐	☒ A clear description of statistics including central tendency (e.g. median, mean) and variation (e.g. standard deviation, interquartile range)
☐	☒ Clearly defined error bars in all relevant figure captions (with explicit mention of central tendency and variation)

See the web collection on statistics for biologists for further resources and guidance.

Software

Policy information about availability of computer code

7. Software

Describe the software used to analyze the data in this study.

All data with the following exceptions were analyzed with GraphPad Prism 7.0.
Crystal Structure Data were collected at ALS 5.1 and 5.2 and processed using HKL2000. Refinement of structures was done using Phenix.
Molecular Dynamics: Visual Molecular Dynamics (VMD http://www.ks.uiuc.edu/Research/vmd/) and GROMACS (http://www.gromacs.org) for the trajectory analysis
UCSF Chimera (https://www.cgl.ucsf.edu/chimera/) for hydrogen bonding analysis mdtraj, scikit, and graphed the output with matplotlib for the principal component analysis (PCA).

For manuscripts utilizing custom algorithms or software that are central to the paper but not yet described in the published literature, software must be made available to editors and reviewers upon request. We strongly encourage code deposition in a community repository (e.g. GitHub). *Nature Methods* guidance for providing algorithms and software for publication provides further information on this topic.

Materials and reagents

Policy information about availability of materials

8. Materials availability

Indicate whether there are restrictions on availability of unique materials or if these materials are only available for distribution by a third party.

There are no restrictions on the availability of unique materials.

9. Antibodies

Describe the antibodies used and how they were validated for use in the system under study (i.e. assay and species).

Staining panel for isolating memory B cells included: anti-CD3-BV510 (BioLegend), CD8-BV510 (BioLegend), CD14-BV510 (BioLegend), CD56-BV510 (BioLegend), CD19-ECD (Beckman), CD27-QD605 (Invitrogen), CD21-Cy5PE (Becton Dickenson), CD38-Alexa Fluor 680 (Becton Dickenson), IgD-Cy7PE (Becton Dickenson), IgM-Cy5.5-PerCP (Becton Dickenson), and IgG-Cy7PE (Becton Dickenson).
For identifying and sorting plasmablasts, the following antibodies were used: CD20-Cy7APC (BD Bioscience), CD19-FITC (BD Bioscience), CD3-Cy7PE (BD Bioscience), CD38-PE (BD Bioscience), and CD27-APC (ThermoFisher).

10. Eukaryotic cell lines

a. State the source of each eukaryotic cell line used.

Expi293 cells were obtained from GIBCO, and GnTI- cells were from ATCC. Both cell lines were used for expression of antibodies.

b. Describe the method of cell line authentication used.

All of the cell lines used were obtained commercially with a certificate of analysis

c. Report whether the cell lines were tested for mycoplasma contamination.

All cell lines tested negative for mycoplasma

d. If any of the cell lines used are listed in the database of commonly misidentified cell lines maintained by ICLAC, provide a scientific rationale for their use.

No commonly misidentified cell lines were used.

Animals and human research participants

Policy information about studies involving animals; when reporting animal research, follow the ARRIVE guidelines

11. Description of research animals

Provide all relevant details on animals and/or animal-derived materials used in the study.

For in vivo studies using the transgenic Plasmodium berghei sporozoites with P falciparum CSP, PbfCSP sporozoites: C57BL/6 mice, female litter-mates, age 6-8wks, were used.
For in vivo studies using the Plasmodium falciparum sporozoites, Human hepatocyte donor-matched FRG huHep mice (both male and female, >4 months of age) were purchased from Yecuris, Inc.

Naive C57BL/6 mice and FRG-Hu Hep mice were used in these studies in accordance with AALAC and IACUC approval and standards at each institution as outlined in methods.

Policy information about studies involving human research participants

12. Description of human research participants

Describe the covariate-relevant population characteristics of the human research participants.

The memory B cell derived monoclonal antibodies characterized in this manuscript were isolated from blood of a normal human volunteer that was enrolled in VRC 312, a human clinical trial (https://clinicaltrials.gov; NCT01441167) that was assessing the safety, immunogenicity and efficacy of an attenuated malaria vaccine (PfSPZ Vaccine).

Plasmablast PfCSP mAbs were isolated from 2 volunteers in the VRC 314 clinical trial (https://clinicaltrials.gov; NCT02015091), an open-label evaluation of the safety, tolerability, immunogenicity and protective efficacy of PfSPZ Vaccine.

Nature Medicine: doi:10.1038/nm.4512